Journal of Virological Methods 151 (2008) 242–248

Contents lists available at ScienceDirect

Journal of Virological Methods

journal homepage: www.elsevier.com/locate/jviromet

Establishment of a feline astrocyte-derived cell line (G355-5 cells) expressing feline CD134 and a rapid quantitative assay for T-lymphotropic feline immunodeficiency viruses

Mieko Ishikawa[a,b], Masaya Okada[a], Kenji Baba[a], Takayuki Shojima[a], Masayuki Shimojima[c], Tomoyuki Miura[b,d], Takayuki Miyazawa[a,*]

[a] Laboratory of Viral Pathogenesis, Center for Emerging Virus Research, Institute for Virus Research, Kyoto University, 53 Shogoin-Kawaracho, Sakyo-ku, Kyoto 606-8507, Japan
[b] Graduate School of Human and Environmental Studies, Kyoto University, Yoshida-Nihonmatsucho, Sakyo-ku, Kyoto 606-8501, Japan
[c] Division of Virology, Department of Microbiology and Immunology, Institute of Medical Science, The University of Tokyo, Minato-ku, Tokyo 108-8639, Japan
[d] Laboratory of Primate Model, Experimental Research Center for Infectious Diseases, Institute for Virus Research, Kyoto University, 53 Shogoin-Kawaracho, Sakyo-ku, Kyoto 606-8507, Japan

ARTICLE INFO

Article history:
Received 2 March 2007
Received in revised form 22 April 2008
Accepted 8 May 2008
Available online 27 June 2008

Keywords:
FIV
Titration
CD134
Astrocytes
Cats

ABSTRACT

Few laboratory strains of feline immunodeficiency virus (FIV) can infect Crandell feline kidney cells (an epithelial-type of cells), however, most primary isolates are T-lymphotropic. T-lymphotropic FIV requires both feline CD134 (an activation marker of helper T-lymphocytes) and CXCR4 (a chemokine receptor) in infection as primary and secondary receptors, respectively. Using feline T-lymphoblastoid cell lines, titration of primary FIV isolates was carried out, however the titration assay was laborious and time-consuming. In this study, using G355-5 cells (a feline astrocyte-derived cell line) transduced with a cDNA of feline CD134 as target cells, an assay system was developed to quantitate primary FIV isolates. With a previous method using a feline T-lymphoblastoid cell line (MYA-1 cells) highly sensitive to FIV, it took 12 days to complete the assay, however, it took only 2 days with the new method. The FIV-infected cells became in a state of persistent infection, producing a large amount of FIV, indicating that the cells will be useful for propagation of T-lymphotropic FIV strains.

1. Introduction

Feline immunodeficiency virus (FIV), an etiological agent of acquired immunodeficiency syndrome in cats, is classified in the genus *Lentivirus* which includes human immunodeficiency viruses (Bendinelli et al., 1995; Pedersen et al., 1987). Based on receptor usage during infection, FIV isolates can be divided into two groups; those that utilize CXCR4 only, and those that utilize feline CD134 (fCD134) as a primary receptor in addition to CXCR4 (Shimojima et al., 2004). Few laboratory strains, such as Petaluma and UT113, belong to the former group, and can infect Crandell feline kidney (CRFK) cells (epithelial-type of cells) (Phillips et al., 1990; Verschoor et al., 1995; Yamamoto et al., 1988), whereas most primary isolates belong to the latter group (Miyazawa et al., 1991; Shimojima et al., 2004; Willett et al., 2006). Although CXCR4 is expressed in a wide variety of cell-types, the expression of CD134 is limited to immune cells, and is induced strongly in CD4-positive T-lymphocytes through antigenic stimulation (Salek-Ardakani and Croft, 2006). Therefore, most primary isolates that use fCD134 as a primary receptor infect predominantly activated T-lymphocytes and do not infect fCD134-negative adherent cells such as fibroblasts and epithelial-type cells including CRFK cells.

By using feline T-lymphoblastoid cell lines, titration of primary FIV isolates has been conducted in different laboratories (Kawaguchi et al., 1990; Matteucci et al., 1995), however the procedure of titration is laborious and time-consuming. The viral titers determined by different methods could not be compared directly. Therefore, an easy method to titrate primary FIV isolates using adherent cells is required. Previously, AH927 (feline fibroblasts) and CRFK cells transduced with fCD134 were shown to be susceptible to FIV primary isolates. However, the cells did not support FIV replication well (Shimojima et al., 2004; Miyazawa et al., unpublished observation). In the present study, a feline astrocyte-derived cell line, G355-5 cells, was found to be very sensitive to T-lymphotropic FIV isolates by expressing fCD134 on the cells. The cells allowed viral proliferation and led to a state of persistent infection, producing large amounts of FIV. Using the cells, an assay that can quantitate FIV primary isolates in only 2 days was established.

* Corresponding author. Tel.: +81 75 751 4814; fax: +81 75 751 4814.
E-mail address: takavet@goo.jp (T. Miyazawa).

0166-0934/$ – see front matter © 2008 Elsevier B.V. All rights reserved.
doi:10.1016/j.jviromet.2008.05.019

2. Materials and methods

2.1. Cells

All cell lines used in this study were grown at 37 °C in a humidified atmosphere of 5% CO_2 in air. G355-5 cells (a feline fetal astrocyte cell line) (Gavrilin et al., 2002; Haapala et al., 1985; Phillips et al., 1990) were grown in Dulbecco's modified Eagle's medium (DMEM) (Sigma–Aldrich, Tokyo, Japan) supplemented with 10% heat inactivated fetal calf serum (FCS) and penicillin (100 units/ml) and streptomycin (100 μg/ml) (Invitrogen, Carlsbad, CA, USA). An interleukin-2 (IL-2) dependent feline T-lymphoblastoid cell line, termed MYA-1 cells (Miyazawa et al., 1989b), was cultured in RPMI 1640 medium (Sigma–Aldrich) supplemented with 10% FCS, 100 units/ml of recombinant human IL-2, 50 μM mercaptoethanol, penicillin (100 units/ml) and streptomycin (100 μg/ml). A potent retrovirus packaging cell line, Plat-E cells (Morita et al., 2000), was grown in DMEM growth medium supplemented with 10 μg/ml of Blasticidin (InvivoGen, San Diego, CA, USA) and 1 μg/ml puromycin (InvivoGen).

2.2. Establishment of G355-5/fOX40 cells

G355-5 cells were transduced with a cDNA encoding fCD134 to establish the cells expressing fCD134. For transduction of fCD134, Plat-E cells were cotransfected with 100 ng of an expression plasmid of fCD134 (pMXpuro-fOX40) (Shimojima et al., 2004) and 900 ng of pCAG-VSV-G (an expression plasmid of vesicular stomatitis virus G protein (VSV-G)) by using FuGENE6 Transfection Reagent (Roche Diagnositics GmbH, Mannheim, Germany). The supernatants containing pseudotype virus bearing VSV-G protein and the fCD134 gene as RNA genome were collected at 2 days post-transfection. G355-5 cells were inoculated with the pseudotype virus, selected with 1 μg/ml of puromycin (InvivoGen) for 2 weeks, and then the selected cells were established as G355-5/fOX40 cells. The G355-5/fOX40 cells were grown in DMEM growth medium supplemented with 1 μg/ml of puromycin throughout the experiments.

2.3. Flow cytometric analysis

G355-5/fOX40 cells detached by trypsinaization were incubated in the staining solution (2% FCS in phosphate-buffered saline (PBS)) with mouse monoclonal antibodies (MAbs), BerACT35 (anti-human CD134)(Ancell Corporation, Bayport, MN, USA), 7D6 (anti-fCD134) (Willett et al., 2007) or F48 (anti-FIV p24) (Nishino et al., 1992) on ice for 30 min. The cells were washed twice with PBS and reacted with a rat anti-mouse IgG1 conjugated with phycoerythrin (COSMO BIO Co., Tokyo, Japan) as the secondary antibody in the same way. The expression of fCD134 on the G355-5/fOX40 cells was analyzed by FACSCalibur flow cytometer (Becton Dickinson (BD), Tokyo, Japan) with Cell Quest™ software (BD Biosciences, San Diego, CA, USA).

2.4. Viruses

FIV strain TM2 (clone 219) (subtype B) was prepared from the culture supernatant of G355-5 cells transfected with an infectious molecular clone of the strain, termed pTM219 (Kiyomasu et al., 1991; Maki et al., 1992). FIV strains TM2 (subtype B) (Miyazawa et al., 1989a), TM2 (clone 219), CABCPaddy00C (subtype C) (Diehl et al., 1995), Shizuoka (subtype D) (Kakinuma et al., 1995) and LP20 (subtype E) (Yamada et al., 1995) were propagated in MYA-1 cells infected with each strain. FIV strain Petaluma (subtype A) was prepared from the culture supernatant of an FIV producer cell line FL4 (Yamamoto et al., 1991). All stock viruses were filtered through a 0.45 μm filter unit (Acrodisc; PALL Corporation, Ann Arbor, MI, USA) and kept at −80 °C until used.

2.5. Sensitivity of G355-5/fOX40 cells to a lymphotropic FIV

G355-5 and G355-5/fOX40 cells were plated in a 12.5 cm_2 tissue culture flask (BD FALCON, Franklin, NJ, USA) at a concentration of 2×10^5 cells in 2 ml, and incubated at 37 °C in a CO_2 incubator for 24 h prior to the viral inoculation. After removal of the culture medium, FIV strain TM2 (clone 219) was inoculated onto each cell line in the presence of 8 μg/ml (final concentration) of polybrene® (hexadimethrine bromide) (Sigma–Aldrich, St. Louis, MO, USA). After incubation for 2 h for viral adsorption, the viral inocula were removed, and cells were washed once with PBS. Four milliliters of DMEM growth medium was added to each flask. At 6 days post-infection, the cells were transferred to a collagen (type I)-coated 96-multiwell plate (Asahi Techno Glass Co., Tokyo, Japan) incubated for 24 h, and then FIV antigens were detected by indirect immnofluorescent assay. The cells were reacted with the F48 MAb (anti-FIV p24 (capsid)) (Nishino et al., 1992) as the first antibody, and 200-fold diluted fluorescein isothiocyanate (FITC)-conjugated AffiniPure donkey anti-mouse IgG (Jackson ImmnoResearch, West Grove, PA, USA) as the secondary antibody. Then the stained cells were observed with IX72 UV microscope (Olympus Co., Tokyo, Japan). Simultaneously, the DNA was extracted from the cells using the QIAamp DNA blood kit (QIAGEN, Inc., Valencia, CA, USA) and analyzed by polymerase chain reaction (PCR) using specific primers for TM2 polymerase (*pol*) gene as described previously (Momoi et al., 1993). In addition, the cells were subjected to immunoblot analysis at 47 days post-infection. Briefly, the cell were washed with PBS twice, then lysed with 1 ml of cell lysis buffer (150 mM NaCl, 1.0% Igepal CA-630, 0.5% sodium deoxycholate, 0.1% SDS, 50 mM Tris) per 10^6 cells and incubated for 15 min on an orbital shaker. The lysed cells were collected and centrifuged for 10 min at 12,000 × *g* to pellet the cellular debris. The supernatants containing cellular proteins were separated by 10% sodium dodecyl sulfate-polyacrylamide gel electrophoresis, transferred to Invitrolon™ PVDF Filter Paper Sandwich (Invitrogen) and then blocked with 10% skim milk in Tris-buffered saline-T (137 mM NaCl, 2.68 mM KCl, 25 mM Tris, 10% Tween20) overnight at 4 °C. Immunodetection was carried out with the F48 MAb, followed by the secondary antibody, anti-digoxigenin conjugated with peroxidase. To visualize proteins reacted with the antibody, the chromogenic reaction was carried out by using Super Signal West Femto Luminol (PIERCE, Rockford, IL, USA). The signals were detected and analyzed by LAS3000 luminescent image analyzer (Fuji film, Tokyo, Japan).

2.6. Titration of FIV on G355-5/fOX40 cells

To quantitate various FIV strains, G355-5/fOX40 cells were plated in a collagen (type I)-coated 96-multiwell plate (Asahi Techno Glass Co.) at a concentration of 6.0×10^3 cells in 200 μl per well. The cells were incubated at 37 °C in a CO_2 incubator for 24 h prior to the viral inoculation. After removal of the culture medium, 50 μl of viral samples diluted serially 10-fold were inoculated per well in quadruplicate in the presence of 8 μg/ml (final concentration) of polybrene® (hexadimethrine bromide) (Sigma–Aldrich). After incubation for 2 h for viral adsorption, the viral samples were removed and the cells were washed once with 50 μl of FCS-free DMEM. Two hundred microliters of DMEM growth medium was added to each well. At the different time points indicated in Fig. 3, the cells were washed with FCS-free medium once, and fixed with cold acetone–methanol (1:1) for 15 min on ice after which the acetone–methanol was replaced with PBS. The plates were kept

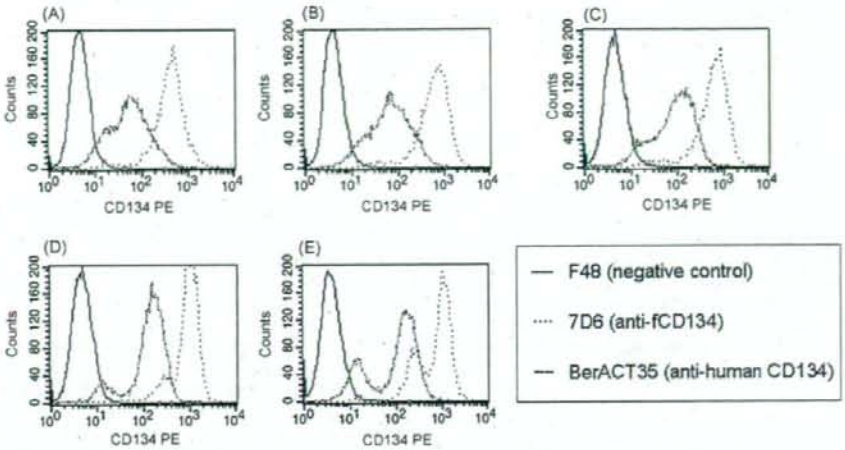

Fig. 1. Expression of fCD134 on G355-5/fOX40 cells. G355-5/fOX40 cells at passage 1 (A), 10 (B), 20 (C), 30 (D) and 40 (E) were reacted with MAbs 7D6 (anti-fCD134), BerACT35 (anti-human CD134) or F48 (anti-FIV p24) as described in Section 2.

at 4 °C until immuno-staining. To detect FIV antigens in the cells, the PBS in the wells was removed and 50 μl of a 100-fold diluted anti-FIV cat serum was added to each well, and then the plates were incubated at 37 °C for 1 h in a humidified atmosphere. The anti-FIV serum was obtained from a specific pathogen-free cat inoculated with FIV strain TM1 (Miyazawa et al., 1989a). After three washes with PBS, 50 μl of a 200-fold diluted goat anti-cat IgG conjugated with FITC (Cappel Biomedical Co., Matvern, PA, USA) was added to each well and the plates were incubated at 37 °C for 1 h in a humidified atmosphere. After another three washes with PBS, the stained

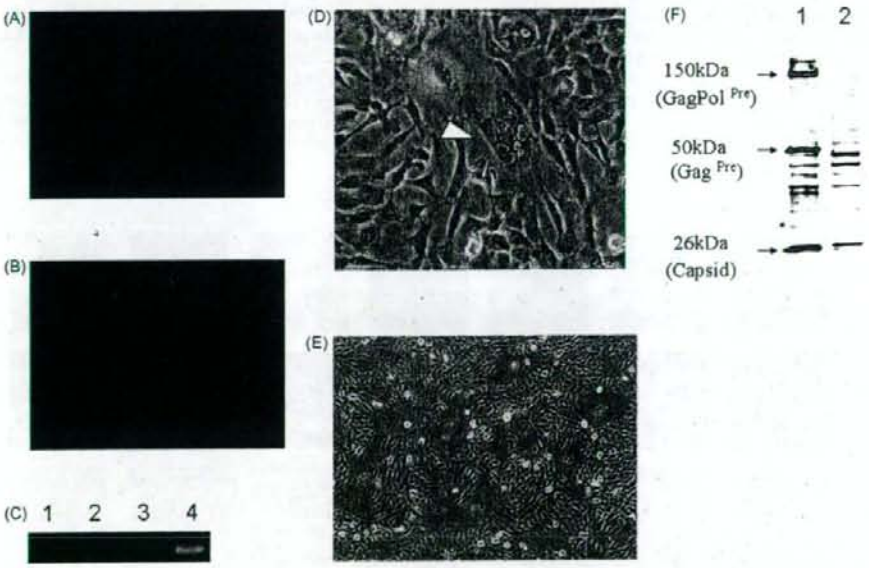

Fig. 2. Sensitivity of G355-5/fOX40 cells to T-lymphotropic FIV strain TM2 (clone 219). G355-5 and G355-fOX40 cells were inoculated with TM2 derived from an infectious molecular clone pTM219 and FIV antigens were detected by indirect immunofluorescent assay. Photographs of G355-5 (A) and G355-5/fOX40 cells (B) at 7 days post-inoculation are shown. (C) Detection of TM2 proviral DNA in TM2 infected cells at 6 days post-inoculation. PCR test was performed using specific primers for TM2 in genomic DNAs prepared from mock-infected G355-5 (lane 1), TM2-inoculated G355-5 (lane 2), mock-infected G355-5/fOX40 (lane 3), and TM2-inoculated G355-5/fOX40 cells (lane 4). (D) CPE characterized by the formation of syncytia appeared in G355-5/fOX40 cells. The white arrowhead indicates prominent syncytia (×400). (E) Appearance of G355-5/fOX40 cells persistently infected with FIV strain TM2. A photograph of the cells at 33 days post-inoculation is shown (×100). (F) Immunoblot analysis of G355-5/fOX40 cells persistently infected with FIV strain TM2 at 47 days post-inoculation (lane 1) and mock-infected G355-5/fOX40 cells (lane 2) using anti-FIV p24 (capsid) MAb F48. The luminescent signals were detected and analyzed by LAS3000 luminescent image analyzer. Three positive bands with strong signals (displayed in pink by the analyzer due to the strong signal and shown in grey here) are indicated by arrowheads.

cells were observed with IX72 UV microscope (Olympus Co.). The 50% tissue culture infective dose ($TCID_{50}$) was calculated by the method of Kärber (1931).

2.7. Titration of FIV on MYA-1 cells

To quantitate FIV on MYA-1 cells, the cells were plated in a 48-multiwell plate at a concentration of 2.4×10^5 cells in 600 μl per well. The cells were incubated at 37 °C in a CO_2 incubator for 24 h prior to the viral inoculation. One hundred microliters of serially diluted (10-fold) viral samples was inoculated to each well in quadruplicate in the presence of 2 μg/ml of polybrene®. At 13 days post inoculation, the cells were collected by centrifugation, smeared on glass slides and then fixed with acetone. FIV antigens were detected by immnofluorescent assay using 100-fold diluted F48 MAb and 200-fold diluted FITC-conjugated AffiniPure donkey anti-mouse IgG (Jackson ImmnoResearch).

2.8. Enzyme-linked immunosorbent assay (ELISA)

To compare the amounts of FIV p24 antigens (capsid) produced in culture supernatants of MYA-1 and G355-5/fOX40 cells infected with TM2 strain (clone 219), a commercial ELISA kit (PetCheck FIV Antigen Test Kit; IDEXX Corp., Portland, ME, USA) was used according to the manufacturer's instruction.

3. Results

3.1. Establishment of G355-5/fOX40 cells

G355-5 cells were transduced with fCD134 gene as described in Section 2. Expression of fCD134 on G355-5/fOX40 cells was assessed by flow cytometry with MAbs BerACT35 (anti-human CD134) and 7D6 (anti-fCD134). Both MAbs detected fCD134, however 7D6 reacted with the molecule stronger than BerACT35 (Fig. 1). The expression of fCD134 was maintained on the G355-5/fOX40 cells that had been passaged 40 times (over 80 days), although a population that expresses fCD134 at a lower level expanded at passage 40. G355-5/fOX40 cells grew slower than G355-5 cells possibly due to the presence of puromycin in the medium. The doubling times of G355-5 and G355/fOX40 cells were 17.1 and 26.0 h, respectively.

3.2. Susceptibilities of G355-5/fOX40 cells to T-lymphotropic FIV strain TM2

To examine the susceptibility of G355-5/fOX40 cells to T-lymphotropic FIV, G355-5 and G355-5/fOX40 cells were inoculated with strain TM2 (clone 219) (Kiyomasu et al., 1991). At 6 days post-inoculation, FIV-specific antigens were detected in G355-5/fOX40 but not in G355-5 cells by the indirect immunofluorescent assay (Fig. 2A and B), and at 6 days post-inoculation, FIV proviral DNA was confirmed by PCR (Fig. 2C). The TM2-infected G355-5/fOX40 cells showed mild cytopathic effect (CPE) of syncytia-formation from 4 days post-inoculation (Fig. 2D). TM2-infected G355-5/fOX40 cells were maintained for over 60 days without coculturing with uninfected cells, accompanied by the CPE of syncytia-formation (Fig. 2E). The percentage of FIV-positive cells reached 80% at 30 days post-inoculation (data not shown), and FIV precursor proteins and its cleaved protein (capsid) were detected by immunoblot analysis using anti-FIV p24 MAb at 47 days post-inoculation (Fig. 2F). The FIV-infected cells produced large amount of FIV, as described in the section of 3.5.

3.3. Titration of T-lymphotropic FIV on G355-5/fOX40 cells

To quantitate T-lymphotropic FIV, serially diluted (10-fold) strain TM2 (parental strain) was inoculated onto G355-5/fOX40 cells in a 96-multiwell plate (Asahi Techno Glass Co.) in quadruplicate. FIV-specific antigens were detected from 24 h post-noculation in wells inoculated with non-diluted and 10-fold diluted viral samples (data not shown). However, the signals were very weak in wells inoculated with samples diluted at further dilutions and it was difficult to distinguish positive signals from non-specific fluorescence (Fig. 3). At 36 h post-inoculation, the FIV antigen-positive fluorescent signals became strong, and the end-point of the dilutions that gave positive fluorescence could be determined. The G355-5/fOX40 cells in each well were nearly confluent at 36 h

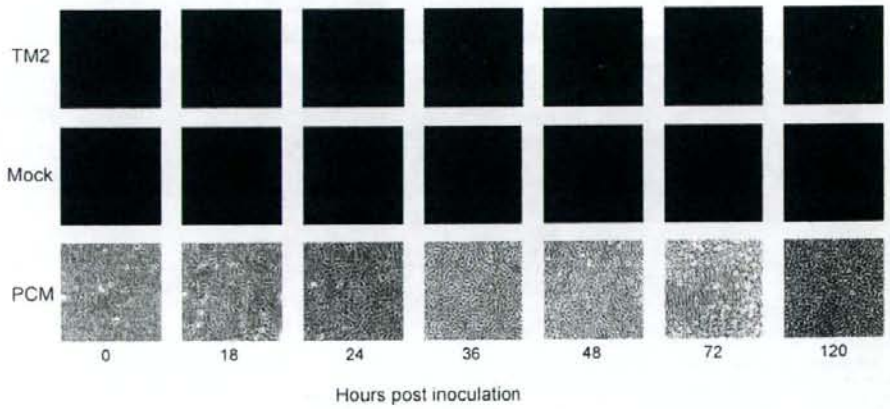

Fig. 3. Expression of FIV antigen in G355/fOX40 cells inoculated with FIV strain TM2 (upper panel). Serially diluted (10-fold) stock viruses (50 μl) were inoculated into the wells of a 96-multiwell plate. The infected cells were fixed with acetone/ethanol at 0, 18, 24, 36, 48, 72 and 120 h post-inoculation and the FIV antigen was detected by indirect immunofluorescence staining using an anti-FIV cat serum. Photographs of cells in the wells inoculated with 100-fold diluted stock viruses taken under IX72 UV microscope (Olympus Co.) are shown. Mock-infected G355/fOX40 cells incubated for the indicated periods are also shown as negative controls in the middle panel. Photographs of mock-infected G355-5/fOX40 cells taken under a phase-contrast microscope (PCM) (CKX41, Olympus Co.) are shown in the lower panel.

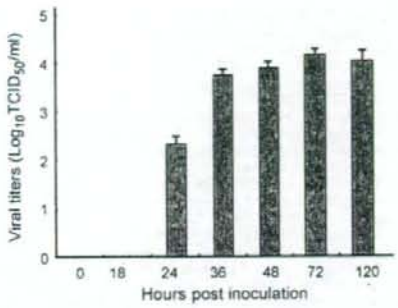

Fig. 4. FIV titers determined after different incubation periods. The end-point dilutions that gave FIV-positive fluorescence were judged at the time points indicated, and the titers are expressed as $TCID_{50}$ per milliliter. Three independent experiments were conducted in quadruplicate and the averages with standard deviations are shown.

post-inoculation forming a uniform monolayer, however the monolayer shrank and was distorted at 72 h post-inoculation due to overgrowth (Fig. 3). Therefore, the cells in each well had to be passaged at 72 h post-inoculation to maintain the cells. The viral titers expressed as $TCID_{50}$ reached a plateau at 36 h post-inoculation (Fig. 4). From these data, we conclude that one can determine the viral titers expressed as $TCID_{50}$ at 48 h post-inoculation in this assay.

3.4. Comparison of the new titration method with the previous method

The viral titer of strain TM2 determined by the new method was compared with that by the previous method. The same virus stock of the strain TM2 was serially diluted (10-fold) and then inoculated onto MYA-1 cells in quadruplicate as described in Section 2. The titer was $10^{4.5}$ $TCID_{50}$/ml which was almost the same with the titer ($10^{4.0}$ $TCID_{50}$/ml) determined by the new method (Fig. 4). Therefore, the new titration method was considered to be as sensitive as the previous method for quantitating T-lymphotropic FIV.

3.5. Application of the new titration method to different subtypes

To assess whether other strains of FIV belonging to different subtypes (A–E) can be quantitated by the new titration method, G355-5/fOX40 cells were inoculated with various FIV strains of different subtypes, and viral titers were determined. All FIV strains infected G355-5/fOX40 cells, and the virus titers were registered at relatively high values (Table 1). These data indicate that the assay is applicable for quantitation of all subtypes of FIV. In addition, the viral titer in the culture supernatant of G355-5/fOX40 cells infected persistently with TM2 (clone 219) (designated as G355-5/fOX40/TM219 cells) was determined. The cells produced FIV reaching to $10^{5.0}$ $TCID_{50}$/ml. To compare the amounts of FIV antigens in the culture supernatants of G355-5/fOX40/TM219 and MYA-1 cells infected with strain TM2 (clone 219), an ELISA to detect FIV p24 antigens was carried out. The optical density values (average (±standard deviation)) of the culture supernatants (5-fold diluted) of the G355-5/fOX40/TM219 and MYA-1/TM219 cells were 2.390 (±0.691) and 0.713 (±0.0382), respectively. These data indicate that G355-5/fOX40 cells produce larger amounts of FIV antigens than MYA-1 cells.

Table 1
Titers of stock viruses of various FIV strains belonging to different subtypes

FIV strains (subtype)	Cells	Viral titers (log_{10} $TCID_{50}$/ml)
Petaluma (A)	FL4	3.1
TM2 (parental) (B)	MYA-1	4.0
TM2 (clone 219) (B)	MYA-1	4.0
TM2 (clone 219) (B)	G355-5/fOX40	5.0
CABC Paddy00C (C)	MYA-1	4.7
Shizuoka (D)	MYA-1	4.3
LP20 (E)	MYA-1	4.7

Viruses were titrated on G355-5/fOX40 cells.

4. Discussion

The primary isolates of FIV require both fCD134 and CXCR4 molecules to infect cells (Shimojima et al., 2004). They cannot replicate in non-lymphoid cell lines and IL-2-independent feline T-lymphoblastoid cell lines such as 3201 and FeTJ cells, due to the lack of fCD134 expression on the cells. Therefore, to isolate FIV from FIV-infected cats, primary feline peripheral blood mononuclear cells (PBMCs) cultured in the presence of IL-2, or IL-2-dependent feline T-lymphoblastoid cell lines, such as MYA-1 and MEM cells, are used currently (Kawaguchi et al., 1990; Matteucci et al., 1995). By introduction of fCD134, an IL-2-independent feline large granular lymphoma cell line termed MCC cells, and a canine T cell line termed CLL cells became sensitive for replication of T-lymphotropic FIV (Shimojima et al., 2004; Willett et al., 2006). In this study, by introduction of fCD134, feline astrocyte-derived G355-5 cells became sensitive for replication of T-lymphotropic strains of FIV belonging to different subtypes. The fCD134-transduced cells, termed G355-5/fOX40 cells, will be useful for the isolation of T-lymphotropic FIV.

Usually, FIV is highly cytopathogenic in both PBMCs and IL-2-dependent T cell lines (Johnson et al., 1996; Holznagel et al., 1998), therefore it was difficult to maintain the infected cells unless uninfected cells were supplied to the culture. Interestingly, the G355-5/fOX40 cells did not show severe CPE after infection, and do not require co-culture of uninfected cells to maintain the culture. In MYA-1 cells, FIV-infection is associated with suppression of the proliferative response of the cells to exogenous IL-2 due to the down-modulation of IL-2 receptor, and FIV induces apoptosis in the cells (Ohno et al., 1994). In HIV infection, down-regulation of Bcl-2, an anti-apoptotic protein, is associated with T-lymphocyte apoptosis (Regamey et al., 1999). FIV does not induce apoptosis in CRFK cells, however, tumor necrosis factor (TNF)-α signaling can induce apoptosis in the FIV-infected CRFK cells (Ohno et al., 1993). The precise mechanism of the low cytopathogenicity of FIV in G355-5/fOX40 cells is unknown at present. However, it is possible that FIV does not induce apoptotic signals in the G355-5 cells or the cells constitutively express anti-apoptotic proteins such as Bcl-2. The G355-5/fOX40/TM219 cells produced large amount of FIV. Because recombinant human IL-2 is rather expensive to purchase from suppliers, the cells are considered to be useful economically for propagation of FIV antigens for virological use and vaccine development.

To quantitate FIV in samples, a Mg^{2+}-dependent reverse transcriptase activity assay and an ELISA to detect p24 antigens have been developed (Pedersen et al., 1987; Tilton et al., 1990; Yamamoto et al., 1988). However, the values determined by these assays do not indicate infectious viral titers. To measure infectious viruses, Tozzini et al. (1992) developed a syncytium assay that uses a cell line derived from CRFK cells, however, the assay is only applicable to CRFK-adapted laboratory strains. Kawaguchi et al. (1990) also developed a titration assay using MYA-1 cells highly sensi-

tive to primary isolates of FIV, in which FIV-specific antigens were detected by indirect immunofluorescence staining on glass slides smeared with FIV-inoculated cells. This method is applicable to T-lymphotropic primary isolates. However, only a small portion of the cells inoculated with each sample was smeared on the well of a glass slide, and if the number of FIV-positive cells was very small in the wells inoculated with the end-point diluted FIV samples, the positive cells were likely to be overlooked. Therefore, to determine the end-point dilutions, it was necessary to culture the cells for 12 days after their inoculation (Kawaguchi et al., 1990). With the method reported now, all the inoculated cells in the wells of 96-multiwell plates can be observed under the UV microscope, and one can determine the end-point dilutions within 2 days after the viral inoculation. The method is also as sensitive as the previous method by using MYA-1 cells.

Based on previous observations (Kawaguchi et al., 1990), the replication cycle of FIV is estimated as 24 h. In this study, the FIV-antigen positive signals were observed from 18 h post inoculation in the wells inoculated with a high concentration of virus (i.e., undiluted and 10-fold diluted samples), however the signals were not strong enough in the wells inoculated with the end-point diluted virus samples at 18 or 24 h post inoculation. Therefore, we could not determine the exact numbers of FIV-infected cells at the time point corresponding to one generation of the viral life cycle. Further improvements are required to measure infectious FIV in infectious units, such as focus-forming units and plaque-forming units, rather than as the $TCID_{50}$.

In summary, an adherent cell line sensitive to primary isolates of FIV was established and a simple quantitative assay for the isolates was developed. The FIV-infected cells become a persistent infection, producing large amounts of FIV. The G355-5/fOX40 cells will be useful for isolation and propagation of FIV.

Acknowledgements

We thank Prof. Toshio Kitamura (University of Tokyo, Tokyo, Japan), Prof. Janet Yamamoto (University of Florida, Gainesville, FL, USA), Dr. Masakazu Hattori (Kyoto University, Kyoto, Japan), and Dr. Masami Mochizuki (Kyoritsu Seiyaku Co., Tokyo, Japan) for providing Plat-E, FL4, Ltk$^-$IL-2.23, and G355-5 cells, respectively. We are also grateful to Prof. E.A. Hoover (Colorado State University, Fort Collins, CO, USA), Prof. Tsutomu Hohdatsu (Kitasato University, Towada, Aomori, Japan) for providing FIV strains CABC Paddy00C and Shizuoka, respectively. We also thank Dr. Brian Willett (Glasgow University, Glasgow, Scotland, UK) and Prof. Kazuyoshi Ikuta (Osaka University, Suita, Osaka, Japan) for providing MAbs 7D6 and F48, respectively. This study was supported in part by Grants-in Aid for Scientific Research from the Japan Society for the Promotion of Science and by Kyoritsu-Seiyaku Co. (Tokyo, Japan).

References

Bendinelli, M., Pistello, M., Lombardi, S., Poli, A., Garzelli, C., Matteucci, D., Ceccherini-Nelli, L., Malvaldi, G., Tozzini, F., 1995. Feline immunodeficiency virus: an interesting model for AIDS studies and an important cat pathogen. Clin. Microbiol. Rev. 8, 87–112.

Diehl, L.J., Mathiason-Dubard, C.K., O'Neil, L.L., Obert, L.A., Hoover, E.A., 1995. Induction of accelerated feline immunodeficiency virus disease by acute-phase virus passage. J. Virol. 69, 6149–6157.

Gavrilin, M.A., Mathes, L.E., Podell, M., 2002. Methamphetamine enhances cell-associated feline immunodeficiency virus replication in astrocytes. J. Neurovirol. 8, 240–249.

Haapala, D.K., Robey, W.G., Oroszlan, S.D., Tsai, W.P., 1985. Isolation from cats of an endogenous type C virus with a novel envelope glycoprotein. J. Virol. 53, 827–833.

Holznagel, E., Hofmann-Lehmann, R., Leutenegger, C.M., Allenspach, K., Huettner, S., Forster, U., Niederer, E., Joller, H., Willett, B.J., Hummel, U., Rossi, G.L., Schüpbach, J., Lutz, H., 1998. The role of in vitro-induced lymphocyte apoptosis in feline immunodeficiency virus infection: correlation with different markers of disease progression. J. Virol. 72, 9025–9033.

Johnson, C.M., Benson, N.A., Papadi, G.P., 1996. Apoptosis and CD4$^+$ lymphocyte depletion following feline immunodeficiency virus infection of a T-lymphocyte cell line. Vet. Pathol. 33, 195–203.

Kakinuma, S., Motokawa, K., Hohdatsu, T., Yamamoto, J.K., Koyama, H., Hashimoto, H., 1995. Nucleotide sequence of feline immunodeficiency virus: classification of Japanese isolates into two subtypes which are distinct from non-Japanese subtypes. J. Virol. 69, 3639–3646.

Kawaguchi, Y., Miyazawa, T., Tohya, Y., Takahashi, E., Mikami, T., 1990. Quantification of feline immunodeficiency virus in a newly established feline T-lymphoblastoid cell line (MYA-1 cells). Arch. Virol. 111, 269–273.

Kärber, G., 1931. Beitrag zur kollectiven Behandlung Pharmakologische Reihen versuche. Arch. Exp. Pathol. Pharmacol. 162, 480–483.

Kiyomasu, T., Miyazawa, T., Furuya, T., Shibata, R., Sakai, H., Sakuragi, J., Fukasawa, M., Maki, N., Hasegawa, A., Mikami, T., Adachi, A., 1991. Identification of feline immunodeficiency virus *rev* gene activity. J. Virol. 65, 4539–4542.

Maki, N., Miyazawa, T., Fukasawa, M., Hasegawa, A., Hayami, M., Miki, K., Mikami, T., 1992. Molecular characterization and heterogeneity of feline immunodeficiency virus isolates. Arch. Virol. 123, 29–45.

Matteucci, D., Mazzetti, P., Baldinotti, F., Zaccaro, L., Bendinelli, M., 1995. The feline lymphoid cell line MBM and its use for feline immunodeficiency virus isolation and quantitation. Vet. Immunol. Immunopathol. 46, 71–82.

Miyazawa, T., Fukasawa, M., Hasegawa, A., Maki, N., Ikuta, K., Takahashi, E., Hayami, M., Mikami, T., 1991. Molecular cloning of a novel isolate of feline immunodeficiency virus biologically and genetically different from the original U.S. isolate. J. Virol. 65, 1572–1577.

Miyazawa, T., Furuya, T., Itagaki, S., Tohya, Y., Nakano, K., Takahashi, E., Mikami, T., 1989a. Preliminary comparisons of the biological properties of two strains of feline immunodeficiency virus (FIV) isolated in Japan with FIV Petaluma strain isolated in the United States. Arch. Virol. 108, 59–68.

Miyazawa, T., Furuya, T., Itagaki, S., Tohya, Y., Takahashi, E., Mikami, T., 1989b. Establishment of a feline T-lymphoblastoid cell line highly sensitive for replication of feline immunodeficiency virus. Arch. Virol. 108, 131–135.

Morita, S., Kojima, T., Kitamura, T., 2000. Plat-E: an efficient and stable system for transient packaging of retroviruses. Gene Ther. 7, 1063–1066.

Momoi, Y., Matsumoto, Y., Watari, T., Goitsuka, R., Miyazawa, T., Mikami, T., Tsujimoto, H., Hasegawa, A., 1993. Detection of feline immunodeficiency virus proviral DNA in feline peripheral blood mononuclear cells by the nested two-step polymerase chain reaction. Zentralbl. Bakteriol. 279, 274–282.

Nishino, Y., Ohki, K., Kimura, T., Morikawa, S., Mikami, T., Ikuta, K., 1992. Major core proteins, p24s, of human, simian, and feline immunodeficiency viruses are partly expressed on the surface of the virus-infected cells. Vaccine 10, 677–683.

Ohno, K., Nakano, T., Matsumoto, Y., Watari, T., Goitsuka, R., Nakayama, H., Tsujimoto, H., Hasegawa, A., 1993. Apoptosis induced by tumor necrosis factor in cells chronically infected with feline immunodeficiency virus. J. Virol. 67, 2429–2433.

Ohno, K., Okamoto, Y., Miyazawa, T., Mikami, T., Watari, T., Goitsuka, R., Tsujimoto, H., Hasegawa, A., 1994. Induction of apoptosis in a T lymphoblastoid cell line infected with feline immunodeficiency virus. Arch. Virol. 135, 153–158.

Pedersen, N.C., Ho, E.W., Brown, M.L., Yamamoto, J.K., 1987. Isolation of a T-lymphotropic virus from domestic cats with an immunodeficiency-like syndrome. Science 235, 790–793.

Phillips, T.R., Talbott, R.L., Lamont, C., Muir, S., Lovelace, K., Elder, J.H., 1990. Comparison of two host cell range variants of feline immunodeficiency virus. J. Virol. 64, 4605–4613.

Regamey, N., Harr, T., Battegay, M., Erb, P., 1999. Downregulation of Bcl-2, but not of Bax or Bcl-x, is associated with T lymphocyte apoptosis in HIV infection and restored by antiretroviral therapy or by interleukin 2. AIDS Res. Hum. Retroviruses 15, 803–810.

Salek-Ardakani, S., Croft, M., 2006. Regulation of CD4 T cell memory by OX40 (CD134). Vaccine 24, 872–883.

Shimojima, M., Miyazawa, T., Ikeda, Y., McMonagle, E.L., Haining, H., Akashi, H., Takeuchi, Y., Hosie, M.J., Willett, B.J., 2004. Use of CD134 as a primary receptor by the feline immunodeficiency virus. Science 303, 1192–1195.

Tilton, G.K., O'Connor Jr., T.P., Seymour, C.L., Lawrence, K.L., Cohen, N.D., Andersen, P.R., Tonelli, Q.J., 1990. Immunoassay for detection of feline immunodeficiency virus core antigen. J. Clin. Microbiol. 28, 898–904.

Tozzini, F., Matteucci, D., Bandecchi, P., Baldinotti, F., Poli, A., Pistello, M., Siebelink, K.H., Ceccherini-Nelli, L., Bendinelli, M., 1992. Simple in vitro methods for titrating feline immunodeficiency virus (FIV) and FIV neutralizing antibodies. J. Virol. Methods 37, 241–252.

Verschoor, E.J., Boven, L.A., Blaak, H., van Vliet, A.L., Horzinek, M.C., de Ronde, A., 1995. A single mutation within the V3 envelope neutralization domain of feline immunodeficiency virus determines its tropism for CRFK cells. J. Virol. 69, 4752–4757.

Willett, B.J., McMonagle, E.L., Ridha, S., Hosie, M.J., 2006. Differential utilization of CD134 as a functional receptor by diverse strains of feline immunodeficiency virus. J. Virol. 80, 3386–3394.

Willett, B.J., McMonagle, E.L., Logan, N., Spiller, O.B., Schneider, P., Hosie, M.J., 2007. Probing the interaction between feline immunodeficiency virus and CD134 by using the novel monoclonal antibody 7D6 and the CD134 (OX40) ligand. J. Virol. 81, 9665–9679.

Yamamoto, J.K., Ackley, C.D., Zochlinski, H., Louie, H., Pembroke, E., Torten, M., Hansen, H., Munn, R., Okuda, T., 1991. Development of IL-2-independent feline lymphoid cell lines chronically infected with feline immunodeficiency virus: importance for diagnostic reagents and vaccines. Intervirology 32, 361–375.
Yamada, H., Miyazawa, T., Tomonaga, K., Kawaguchi, Y., Maeda, K., Castellano, M.C., Kai, C., Tohya, Y., Mikami, T., 1995. Phylogenetic analysis of the long terminal repeat of feline immunodeficiency viruses from Japan, Argentina and Australia. Arch. Virol. 140, 41–52.
Yamamoto, J.K., Sparger, E., Ho, E.W., Andersen, P.R., O'Connor, T.P., Mandell, C.P., Lowenstine, L., Munn, R., Pedersen, N.C., 1988. Pathogenesis of experimentally induced feline immunodeficiency virus infection in cats. Am. J. Vet. Res. 49, 1246–1258.

Vet Pathol 45:232–235 (2008)

Congenital Cystic Adenomatoid-like Malformation in a Cynomolgus Monkey (*Macaca fascicularis*)

S. Okabayashi, C. Ohno, M. Kato, H. Nakayama, and Y. Yasutomi

Tsukuba Primate Research Center, National Institute of Biomedical Innovation, Ibaraki, Japan (SO, CO, MK, YY); The Corporation for Production and Research of Laboratory Primates, Ibaraki, Japan (SO, CO, MK); and the Laboratory of Veterinary Pathology, Graduate School of Agricultural and Life Sciences, The University of Tokyo, Tokyo, Japan (HN)

Abstract. Congenital cystic adenomatoid malformation (CCAM) is a developmental lung abnormality characterized by abnormal proliferation of mesenchymal elements and failure of bronchiolar structures to mature, ultimately resulting in the compression of normal pulmonary tissue and mediastinal shift with rapid expansion of cysts. Although various clinical and pathologic studies of CCAM in humans exist, CCAM has yet to be reported in animals, even in nonhuman primates. In the present study, histopathologic analyses of a neonatal cynomolgus monkey that died 17 days after birth revealed that normal lung architecture was replaced by disorganized overgrowths of cysts lined with simple cuboidal epithelium. The epithelium projected a few ciliates into the air spaces and produced mucus. To our knowledge, this is the first case study describing CCAM or a CCAM-like lesion in nonhuman primates.

Key words: Congenital cystic adenomatoid malformation; cynomolgus monkey; histopathological analyses; lung.

Congenital cystic adenomatoid malformation (CCAM) is a rare fetal developmental abnormality of the lung. First described by Ch'in and Tang in 1949,[2] it is characterized by abnormal development of terminal respiratory structures, resulting in an adenomatoid proliferation of bronchiolar elements and cyst formation.[11,18,19] CCAM is observed mainly during the neonatal period and infancy and can be diagnosed prenatally by ultrasonography after 16 weeks of gestation.[9,10,13,14] CCAM lesions are believed to be a consequence of abnormal embryogenesis during the first 6 to 7 weeks of pregnacy.[18]

Stoker et al.[18,19] classified CCAM into three types based on clinical and histologic criteria. In the neonatal period, the expansion of cysts and the compression of surrounding lung parenchyma cause progressive respiratory distress.[18,19] Moreover, emphysema-related lung masses also cause dyspnea, eventually leading to death.[18,19] Fetuses with CCAM tend to be born prematurely or are stillborn.[12] Due to the severity and impact of this disorder, numerous clinical and pathologic studies in humans have focused on determining the pathologic mechanisms underlying CCAM and the clinical management of CCAM.[1,4,8,15–17] Although CCAM is well characterized in humans, CCAM or CCAM-like pathogenesis has not been reported in animals. To our knowledge, we report here the first case of CCAM in a nonhuman primate, as demonstrated through histopathologic analyses of a neonatal cynomolgus monkey.

A male cynomolgus monkey (*Macaca fascicularis*) born in our colony died naturally 17 days after birth. The animal was housed in an individual cage with its mother and maintained according to the National Institute of Biomedical Innovation rules and guidelines for experimental animal welfare. The mother monkey had the experience to raise another 6 baby monkeys. In this case, the mother monkey embraced her baby as usual, and the lactation also was observed. After birth, breeding staff members observed the baby monkey to check its health status; however, they could not find any abnormalities until 3 days before it died. Necropsy was performed. Tissues were fixed in 10% neutral-buffered formalin, processed conventionally, embedded in paraffin, cut into 3-μm–thick sections, and stained with hematoxylin and eosin. Lung tissues were also stained with periodic acid–Schiff (PAS), Alcian blue (AB), Masson's trichrome, and elastica van Gieson stains.

For immunohistochemical analyses, sections were first deparaffinized by pretreatment with 0.3% H_2O_2 solution. Next, sections underwent antigen retrieval with citric acid buffer and heating in an autoclave at 121°C for 10 minutes. Finally, sections were incubated free floating in primary antibody solution overnight at 4°C. The primary antibodies were anti-cytokeratin antibody (AE1/AE3 clone; 1:50; Dako, Glostrup, Denmark), anti-vimentin antibody (1:100; Dako), and anti–von Willebrand factor VIII antibody (1:400; Dako). Following brief washes with buffer, the sections were sequentially incubated with Polymer immunocomplex (Dako) for 30 minutes. Immunoreactive elements were visualized by treating the sections with 3-3′ diaminobenzidine tetroxide (Dojin Kagaku, Kumamoto, Japan). The sections then were counterstained with hematoxylin.

Fig. 1. Lung, 17-day-old monkey. The right lower lobe contains a 3.5 cm × 2 cm × 1 cm, thin-walled, multicystic structure filled with air. The remaining lobes were pinkish-red and showed signs of atelectasis. Bar = 5 mm.

Macroscopically, lesions were confined to the right lower pulmonary lobe. In the lesion area, we found a thin-walled multicystic structure (3.5 cm × 2 cm × 1 cm) filled with air (Fig. 1). The other pulmonary lobes were pinkish-red and showed signs of atelectasis (Fig. 1). In heart, both atria dilated with clot. Microscopically, the affected lung displayed diffuse, abnormal architecture composed of numerous large, partially collapsed air spaces. These lesions looked like adenomatoids, and air spaces were lined with simple cuboidal epithelium surrounded by connective tissue and immature cartilage (Fig. 2). Within the air spaces, we found a few ciliates (Fig. 3), and PAS stained a little mucus on a part of epithelium (Fig. 4). AB weakly stained premature cartilage. Masson trichrome stained fibrous interstices, but smooth muscles were not observed. Elastica van Gieson stained elastic fibers around the air spaces. Other lung tissues were congested and were compressed by the surrounding mass. The border between the cystic lesion and normal tissue was not clear. In liver and kidney, congestion was observed.

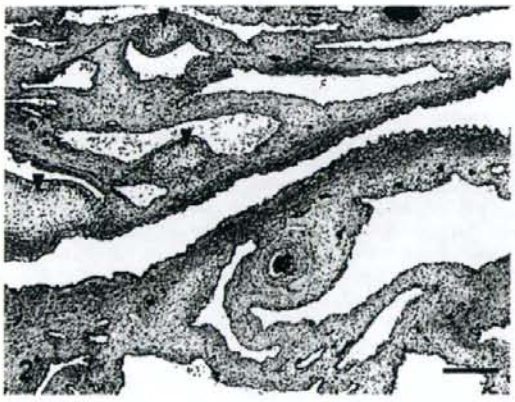

Fig. 2. Lung, 17-day-old monkey. Photomicrograph of affected lung showing diffusely abnormal architecture characterized by numerous large air spaces lined with epithelium surrounded by connective tissue and immature cartilage (arrowheads). HE. Bar = 250 μm.

Fig. 3. Lung, 17-day-old monkey. Air spaces are lined with simple cuboidal epithelium. A few ciliated cells (arrowheads) were observed within some air spaces. HE. Bar = 6 μm.

Immunohistochemical analyses revealed that the epithelium of the lesion was immunopositive for cytokeratin but negative for vimentin and von Willebrand factor VIII. However, the fibrous interstices and premature cartilage of the lesion were immunopositive for vimentin.

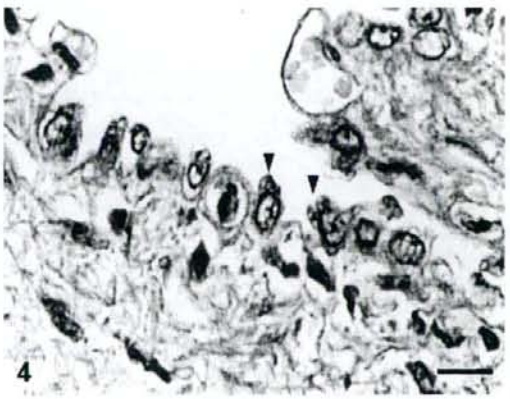

Fig. 4. Lung, 17-day-old monkey. Periodic acid–Shiff demonstrated mucus (arrowheads) on a part of the epithelium lining air spaces. Bar = 8 μm.

The congenital pulmonary abnormalities can be divided into some classifications.[5,6]

1. Bronchopulmonary sequestration:[5,6] bronchopulmonary sequestration is a pulmonary malformation in which a portion of lung parenchyma has no communication with the tracheobronchial tree and receives its blood supply via a systemic artery. The abnormality is observed as intralobar or extralobar. The first type (intralobar sequestration [ILS]) is contiguous with normal lung parenchyma and within the same visceral pleural envelope. The abnormal tissue is usually well demarcated from surrounding lung parenchyma and consists of one or more cystic spaces filled with mucus or pus. Microscopically, they resemble dilated bronchi, with respiratory epithelium and occasional mural cartilage plates. The latter type (extralobar sequestration [ELS]) is enclosed within its own pleural membrane, usually close to a normal lung. In addition to these types, the bronchopulmonary foregut malformation (BPFM)[7] is characterized by the pulmonary sequestrations that communicate with the upper gastrointestinal tract.

2. Bronchogenic cysts:[5,6] Bronchogenic cysts are lesions of congenital origin derived from the primitive foregut and are usually solitary, thin-walled, unilocular, and roughly spherical. They are filled with either mucus or serous fluid, and they do not communicate with the trancheobronchial tree. Microscopically, the cyst wall is lined by respiratory epithelium and contains cartilage, smooth muscle and, sometimes, seromucinous bronchial-type glands.

3. Congenital lobar emphysema (CLE):[5,6] CLE is characterized by severe overinflation of a pulmonary lobe. The pathogenesis is perhaps due to hypoplasia of bronchial cartilage. Microscopically, there is massive distention of alveolar spaces, but not tissue destruction.

4. Congenital cystic adenomatoid malformation (CCAM):[3,5,6,18,19] CCAM consists of an intralobar mass of disorganized pulmonary tissue that can exist with or without gross cyst formation. The anomaly is considered by some to represent a hamartoma, whereas others feel that it results from localized arrested development of the fetal bronchial tree. The cysts can usually be shown to communicate with normal airways; vascularization is by way of the pulmonary circulation. The histologic appearances give rise to the name, as there are numerous spaces of varying size, some of which resemble glandular acini, being lined cuboidal or columnar epithelium. According to the Stocker et al.[18,19] on the basis of 38 cases, CCAM is classified into three categories. Type I consists of some large cysts (>2 cm in diameter). The lesions are lined by ciliated cuboidal or columnar epithelium with elastic tissue or smooth muscle. Mucus-producing cells or cartilage may be present. Relatively normal alveoli may be seen between or adjacent to these cysts. Type II consists of small cysts (<2 cm in diameter) lacking mucus-producing cells and cartilage. Type III consists of bulky, firm, solid mass with small cysts (<0.5 cm in diameter). The lesions are lined with nonciliated cuboidal epithelium.

In this case, we found the abnormal architecture composed of numerous large air spaces. These cysts looked like adenomatoids, and they were lined with simple cuboidal epithelium surrounded by elastic tissue and premature cartilage. These pathologic features are different from that of ILS, ELS, BPFM, bronchogenic cysts, or CLE, because cysts were not unilocular, they did not include mucus or serous fluid, and they had neither abnormal artery nor communication with the upper gastrointestinal tract. Furthermore, the lesions were not massive distentions of alveolar spaces. Taken together, this monkey case is considered CCAM.

We applied the Stocker et al.[18,19] classification scheme to our monkey case, since no reports on CCAM in animals currently exist. In this monkey case, we observed large cysts greater than 2 cm in diameter (Fig. 1) lined with sparsely ciliated epithelium (Fig. 3) that produced a little mucus in a part (Fig. 4). These cysts also contained immature cartilage (Fig. 2). Thus, this monkey case exhibited sufficient pathologic features to meet the criteria for type I CCAM. We considered that pulmonary lobes were compressed by cysts and alveolars were collapsed, so that this monkey would suffer from respiratory distress and die. Moreover, the heart or great vessel may be compressed by pulmonary cysts, so that we consider liver and kidney congestion as a result of circulatory failure.

To our knowledge, this is the first case study describing CCAM or CCAM-like lesions in nonhuman primates. We have no information about the genetic background of the monkey in this case. Nonetheless, this case is quite noteworthy, because it provides an example of CCAM-like pathology in animal tissue. Should we encounter other CCAM-resembling or suspicious cases, we will carry out not only histopathologic analyses but also genetic analyses to determine the genetic background of these monkeys. Accumulating data from such analyses in nonhuman primates will contribute greatly to understanding CCAM pathology.

Acknowledgements

This study was supported by Tsukuba Primate Research Center, National Institute of Biomedical Innovation, Japan.

References

1 Bale PM: Congenital cystic malformation of the lung. A form of congenital bronchiolar ("adenomatoid") malformation. Am J Clin Pathol **71**:411–420, 1979

2 Ch'in KY, Tang MY: Congenital adenomatoid malformation of one lobe of a lung with general anasarca. Arch Pathol **48**:221–229, 1949

3 Cloutier MM, Schaeffer DA, Hight D: Congenital cystic adenomatoid malformation: review. Chest **103**:761–764, 1993

4 Dumez Y, Mandelbrot L, Radunovic N, Revillon Y, Dommergues M, Aubry MC, Aubry JP, Narcy F, Sonigo P: Prenatal management of congenital cystic adenomatoid malformation of the lung. J Pediatr Surg **28:**36–41, 1993
5 Dunnill MS: Pulmonary Pathology, Churchill Livingstone, New York, New York, 1982
6 Scarpelli EM, Auld PAM, Goldman HS, Lea, Febiger: Pulmonary Disease of the Fetus Newborn and Child, Lea & Febiger, Philadelphia, Pennsylvania, 1978
7 Eom DW, Kang GH, Kim JW, Ryu DS: Unusual bronchopulmonary foregut malformation associated with pericardial defect: bronchogenic cyst communicating with tubular esophageal duplication. J Korean Med Sci **22:**564–567, 2007
8 Heydanus R, Stewart PA, Wladimiroff JW, Los FJ: Prenatal diagnosis of congenital cystic adenomatoid lung malformation: a report of seven cases. Prenat Diagn **13:**65–71, 1993
9 Katzenstein AA, Askin FB: Surgical Pathology of Non-neoplastic Lung Disease, 2nd ed., pp. 468–506. W. B. Saunders Co., Philadelphia, PA, 1990
10 Kravitz RM: Congenital malformations of the lung. Pediatr Clin North Am **41:**453–472, 1994
11 Kwittken I, Reiner L: Congenital cystic adenomatoid malformation of the lung. Pediatrics **30:**750–768, 1962
12 Lischka A, Popow C, Horcher E, Kratochwil A, Reiner A: Problems of congenital cystic adenomatoid malformation of the lung in premature babies. Padiatr Padol **17:**465–472, 1982
13 Morelli L, Piscioli I, Licci S, Donato S, Catalucci A, Del Nonno F: Pulmonary congenital cystic adenomatoid malformation, type I, presenting as a single cyst of the middle lobe in an adult: case report. Diagn Pathol **2:**17, 2007
14 Luck SR, Reynolds M, Raffensberger JG: Congenital bronchopulmonary malformation. Curr Probl Surg **23:**245–314, 1986
15 Miller PK, Sieber WK, Yunis EJ: Congenital adenomatoid malformation of the lung. A report of 17 cases and review of the literature. Pathol Annu **15:**387–402, 1980
16 Salle B, Rebaud A, Rudigoz RC, Mellier G: Prenatal diagnosis of adenomatoid malformation of the lung. 5 cases and review of the literature. J Gynecol Obstet Biol Reprod (Paris) **22:**53–57, 1993
17 Singh M, Mitra S, Kumar L, Narang A, Rao KL, Kakkar N: Congenital cystadenomatoid malformation of lung. Indian Pediatr **37:**1269–1274, 2000
18 Stocker JT, Madewell JE, Drake RM: Congenital cystic adenomatoid malformation of the lung. Classification and morphologic spectrum. Hum Pathol **8:**155–171, 1977
19 Stocker JT, Madewell JE, Drake RM: Cystic and congenital lung disease in the newborn. Perspect Pediatr Pathol **4:**93–154, 1978

Request reprints from S. Okabayashi, The Corporation for Production and Research of Laboratory Primates, Hachimandai 1-1, Tsukuba-shi, Ibaraki 305-0843 (Japan) E-mail: okarin@primate.or.jp.

Arch Dermatol Res
DOI 10.1007/s00403-008-0873-y

ORIGINAL PAPER

Administration of Ag85B showed therapeutic effects to Th2-type cytokine-mediated acute phase atopic dermatitis by inducing regulatory T cells

Hitoshi Mori · Keiichi Yamanaka · Kazuhiro Matsuo · Ichiro Kurokawa · Yasuhiro Yasutomi · Hitoshi Mizutani

Received: 5 February 2008 / Revised: 22 May 2008 / Accepted: 20 June 2008

Abstract Increase in the number of patients with atopic dermatitis (AD) has been recently reported. T helper (Th) cells that infiltrate AD skin lesions are Th2-type dominant; reduced exposure to environmental Th1-cytokine-inducing microbes is believed to contribute to the increased number of AD patients. Regulatory type immune responses have been also associated with the occurrence of AD. It has been reported that antigen 85B (Ag85B) purified from mycobacteria is a potent inducer of Th1-type immune response in mice as well as in humans. In this study, we have examined the effect of plasmid DNA encoding Ag85B derived from *Mycobacterium kansasii* on AD skin lesions induced by oxazolone (OX) application. Th2-cytokine mediated mouse AD model with immediate type response followed by a late phase reaction was developed by repeated applications of low-dose OX to sensitized mice. Mice were immunized with plasmid DNA encoding cDNA of Ag85B before OX sensitization or during repeated elicitation phase. Both therapies were associated with significant suppression of immediate type response, clinical appearance, dermal cell infiltration, reduced IL-4 production, and augmented IFN-γ mRNA expression compared to placebo-treated mice. Additionally, increased number of Foxp3$^+$ regulatory T cells were observed in the skin sections in Ag85B treated mice. The results of this study suggest that Ag85B DNA vaccine is a potential therapy for Th2 type dermatitis.

Keywords Atopic dermatitis · Antigen 85B · Regulatory T cell

Abbreviations

AD	Atopic dermatitis
Th	T helper
BCG	*Bacillus Calmette-Güerin*
Treg	Regulatory T cell
Ag85B	Antigen 85B
OX	Oxazolone

Introduction

It is known that acute phase skin lesion in atopic dermatitis (AD) is associated with enhanced secretion of T helper (Th) 2-type cytokines [8]. Increased incidence of atopic disorders has been reported in industrialized countries; according to the hygiene hypothesis, the increase in the incidence of patients may be explained by a better lifestyle and less exposure to environmental microbes [5, 7, 28]. Environmental microbes such as mycobacteria or certain virus may promote Th1-type immune response and thus reducing atopy-associated Th2-type reaction. For instance, the study

H. Mori · K. Yamanaka · I. Kurokawa · H. Mizutani (✉)
Department of Dermatology,
Mie University Graduate School of Medicine,
2-174 Edobashi, Tsu, Mie 514-8507, Japan
e-mail: h-mizuta@clin.medic.mie-u.ac.jp

K. Matsuo
Research and Development Department,
Japan BCG Laboratory, Tokyo, Japan

Y. Yasutomi
Laboratory of Immunoregulation and Vaccine Research,
Tsukuba Primate Research Center,
National Institute of Biomedical Innovation,
Tsukuba, Ibaraki, Japan

Y. Yasutomi
Department of Immunoregulation,
Mie University Graduate School of Medicine,
Tsu, Mie, Japan

carried out in Japanese *Bacillus Calmette-Güerin* (BCG)-vaccinated school children showed that responders to tuberculin had a lower prevalence of atopic disease compared to tuberculin non-responders [28]. BCG-treated mice showed suppression of experimental allergic responses [12]. More recently, it has been shown that microbial stimulation can induce regulatory T (Treg) cells with the ability to suppress both Th1-type and Th2-type inflammation [35]. In the experimental model of pulmonary inflammation, *Mycobacterium vaccae* reduces allergic pulmonary inflammation significantly by increasing the number of Treg cells that secretes IL-10 and TGF-β[37]. These observations indicate that shift from Th2 to Th1 type immune response by mycobacteria may be used for the prevention and treatment of atopic disorders.

The specific antigens eliciting Th1-type immune responses in mycobacteria have not been elucidated so far; a recent study suggested that one of the specific proteins for Th1 development is antigen 85B (Ag85B) [31]. Ag85B is a 30-kDa major protein secreted from all *Mycobacterium* species and that belongs to the Ag85 family[4]. The Ag85B can induce a strong Th1-type immune response in mice as well as in humans [31], and DNA vaccines encoding Ag85B have been reported to protect animals from tuberculosis infection by inducing Th1 response [34, 36]. We have previously reported enhancement of anti-tumor specific CTL response using Ag85B-transfected tumor cells, and by inducing Th1-type immune responses as a vaccine adjuvant [22, 30].

The purpose of the present study was to evaluate the therapeutic efficacy of Ag85B derived from *M. kansasii* in acute phase dermatitis. Repeated applications of hapten such as oxazolone (OX) on BALB/c mice causes delayed type hypersensitivity in the beginning that changes to an immediate-type response in the late phases with elevated IgE production, and deviation of Th cell responses. The skin lesions that appear in late phases are compatible with the clinical findings as well as cytokine profile observed in AD [19, 21]. In all Ag85B-treated AD mice, the immediate type reaction is effectively suppressed and IL-4 is significantly reduced. The results of this study provide evidence for the potential usefulness of Ag85B as a novel approach for the treatment of Th2 type-mediated dermatitis such as AD.

Materials and methods

Animals

Six-week-old BALB/c male mice were purchased from Japan SLC Co. (Shizuoka, Japan) and used at the age of 7 weeks. Animal care was done according to ethical guidelines, and approved by the Institutional Board Committee for Animal Care and Use of Mie University.

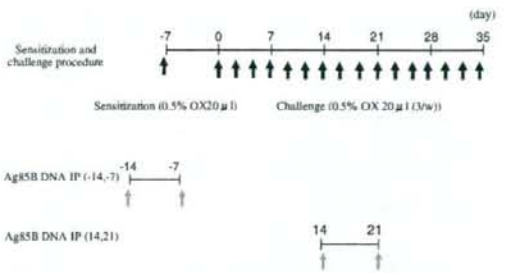

Fig. 1 Model of chronic contact hypersensitivity, and treatment with Ag85B DNA

Sensitization and challenge of animals

Oxazolone was purchased from Sigma (St Louis, MO, USA), and dissolved in acetone/olive oil (1:1). As shown in Fig. 1, mice were initially sensitized by pasting 20 μl of 0.5% OX solution to their left ear 7 days prior to the first challenge (day -7) and then 20 μl of 0.5% OX solution was repeatedly applied on the left ear three times per week from day 0. The ear swelling response was expressed as the difference between before and 30 min after application. The Ag85B expression vector pcDNA-Ag85B of *M. kansasii* open reading frame lacking a signal sequence has been constructed into KpnI–ApaI sites of pcDNA3.1 as described previously [22]. Plasmid DNAs were purified using the Plasmid Mega Kit (Qiagen, Chatsworth, CA, USA). The empty plasmid pcDNA3.1 was used as a control. Plasmid DNAs were diluted with sterilized physiological saline. Hundred micrograms per mouse of plasmid DNA was injected intraperitoneally on day -14, -7 to evaluate prophylactic effects, or on day 14 and 21 for the assessment of therapeutic effects.

Histological analysis

Skin specimens obtained 30 min after the final challenge were fixed in 10% buffered neutral formaldehyde and embedded in paraffin. Sections prepared of 7 μm thickness were stained with hematoxylin and eosin (H&E), or truidine blue.

Immunohistochemistry

The left ear was sacrificed on day 35, and was embedded in Tissue-Tek OCT compound (Miles, Elkhart, USA), frozen in liquid nitrogen, and cut with a cryostat into 7 μm-thick sections. The tissue preparations were then incubated with

primary antibodies specific for Foxp3 (eBioscience, San Diego) overnight, followed by the additional incubation with Alexa Fluor 633 conjugated secondary antibodies (Molecular Probes, Eugene, OR, USA) for 30 min at room temperature. Sections were examined under Fluoview FV1000 laser scanning confocal microscopy (Olympus, Tokyo, Japan). The numbers of $Foxp3^+$ cells were counted in high power fields; five randomly chosen fields were evaluated.

Analysis of cytokine mRNA expression in mouse ears

At 6 h after the final challenge, the left ear skin was sampled. The specimen was homogenized and mRNA was extracted using Isogen (Nippon Gene, Tokyo, Japan) according to the manufacture's instruction; 1 ml of homogenate was vigorously mixed with 200 μl of chloroform, and then centrifuged at 15,000 rpm for 15 min at 4°C. Aqueous phase was separated and mixed with 0.5 ml of 2-propanol (Nacalai Tesque, Kyoto, Japan) to precipitate RNA. After centrifugation, the precipitate was washed with 1 ml of 75% ethanol (Nacalai Tesque) and dried up. RNA was suspended in 50 μl of RNase-free water, the concentration was calculated based on the absorbance at 260 nm, and the quality was confirmed by electrophoresis. cDNA was synthesized from 10 μg of mRNA using archive kit (ABI, Foster City, CA, USA) according to the manufacturer's protocol.

Cytokine mRNA expression in skin

Real time quantitative reverse transcription-polymerase chain reaction (RT-PCR) was performed to measure transcriptional activity in the skin lesions. A 25-μl reaction mixture containing 1 μg total of cDNA, 900 nmol of each primer, and 250 nmol of TaqMan probe were mixed with 12.5 μl of TaqMan Master Mix (ABI, Foster City, CA, USA). The following primers and probes were used for the PCR reactions: mouse IL-4; forward: 5′-ACAGGAGAA GGGACGCCAT-3′, reverse: 5′-GAAGCCCTACAGAC GAGCTCA-3′, probe: 5′-TCCTCACAGCAACGAAGAA CACCACA-3′-TAMRA, IFN-γ; forward: 5′-TCAAGTG GCATAGATGTGGAAGAA-3′, reverse: 5′-TGGCTCT GCAGGATTTTCATG-3′, probe: 5′-TCACCATCCTTTT GCCAGTTCCTCCAG-3′-TAMRA, IL-10; forward: 5′-G GTTGCCAAGCCTTATCGGA-3′, reverse: 5′-ACCTGCT CCACTGCCTTGCT, probe: 5′-TGAGGCGCTGTCGTC ATCGATTTCTCCC-3′-TAMRA, TGF-β; forward: 5′-TG ACGTCACTGGAGTTGTACGG-3′, reverse: 5′-GGTTC ATGTCATGGATGGTGC-3′, probe: 5′-TTCAGCGCTC ACTGCTCTTGTGACAG-3′-TAMRA, β-actin; forward: 5′-AGAGGGAAATCGTGCGTGAC-3′, reverse: 5′-CAA TAGTGATGACCTGGCCGT-3′, probe: 5′-CACTGCCG CATCCTCTTCCTCCC-3′-TAMRA [25]. PCR was performed under the following conditions: 95°C for 10 min, then 40 cycles of 95°C for 15 s, 60°C for 1 min were carried out. Fluorescence data were collected during each annealing-extension step and analyzed by using ABI Prism SDS software version 1.9.1. All samples were normalized for to the β-actin mRNA content.

Measurement of serum IgE

Blood was collected under anesthesia 6 h after the last challenge. Serum IgE levels were determined by a sandwich enzyme-linked immunosorbent assay (BD PharMingen, CA, USA) according to the manufacturer's instructions. Optical density of each well was determined by using a microplate reader (Multiscan JX) (Thermo Electron, Yokohama, Japan). Standard curve was prepared using mouse anti-TNP IgE standard (BD PharMingen, CA, USA) diluted with PBS containing 10% FCS.

Statistical analysis

Differences in ear swelling and serum IgE levels were analyzed by the Kruskal–Wallis test. $P < 0.05$ was taken as significant.

Results

Effect of Ag85B on skin inflammation

We first examined whether Ag85B could modulate ear-swelling reaction in a mouse model of OX-induced AD like skin lesions. Repeated applications of OX cause Th2-mediated immediate type response. Ear swelling was measured with thickness gauge calipers before and 30 min after OX challenge on the pinna of the ear on day 32. In both prophylactic and therapeutic models, the administration of Ag85B significantly suppressed swelling compared to placebo-treated controls (Fig. 2a). The OX-challenged placebo-treated mice showed severe skin inflammation, however administration of Ag85B DNA reduced atopic inflammatory reactions (Fig. 2b).

Histological analysis

Histological examination in OX-challenged mice showed epidermal hyperplasia and strong intraepidermal and intradermal inflammatory cell infiltration including mononuclear cells, neutrophils, and granular cells (Fig. 3a). Both prophylactic and therapeutic administration of Ag85B DNA clearly reduced inflammatory cell infiltration and epidermal thickness. Skin sections stained with truidine blue showed decreased mast cell infiltration in Ag85B-treated mice (Fig. 3b).

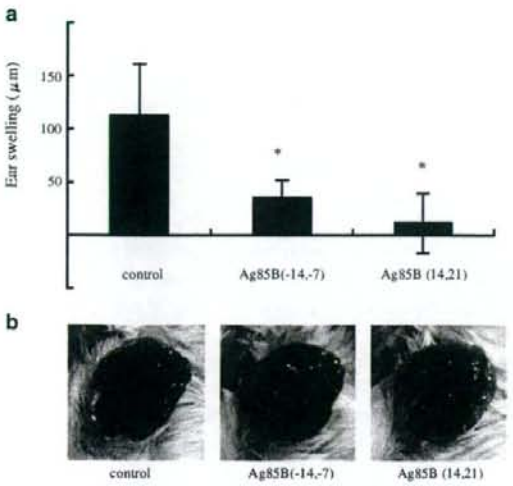

Fig. 2 **a** OX-induced ear swelling. The ear swelling response was expressed as the difference between ear thickness before and 30 min after each application on day 32. The columns and error bars represent mean ± SEM. $^*P < 0.05$. Swelling was suppressed significantly in Ag85B-treated mice compared with those in placebo-treated mice. **b** Clinical features of ear skin on day 35. The OX-challenged mice showed severe skin eruption, however administration of the Ag85B DNA in both prophylactic and therapeutic models clearly reduced atopic inflammatory reactions in OX-sensitized mice

Ag85B treatment shifted the Th1/Th2 balance toward Th1

IFN-γ and IL-12 shift the Th1/Th2 balance toward Th1 condition; while IL-4 and IL-5 are key cytokines in Th2 response [24, 29]. To clarify the type of immune response in skin lesions after treatment with Ag85B, we analyzed the mRNA expression levels of IL-4 and IFN-γ by real time quantitative RT-PCR. The results were normalized to the β-actin mRNA content. As shown in Fig. 4, the expression of IL-4 mRNA was reduced in Ag85B-treated mice in both prophylactic and therapeutic models. On the contrary, the expression of IFN-γ was enhanced in Ag85B-treated mice. These results suggest that the application of Ag85B shifts the immune response toward Th1-predominace.

Total serum IgE levels

Atopic dermatitis is characterized by elevated IgE levels. Repeated applications of OX cause a gradual elevation of antigen-specific IgE level. We analyzed the degrees of IgE levels in sera collected from experimental mice. Administration of Ag85B significantly reduced the serum levels of IgE (Fig. 5).

Ag85B treatment induces regulatory T cells

TGF-β and IL-10 are important regulatory cytokines produced by Treg [11]. To investigate the mechanisms of the therapeutic effectiveness of Ag85B, we examined the mRNA levels of TGF-β and IL-10. As shown in Fig. 6a, TGF-β and IL-10 were significantly increased in Ag85B-treated mice in both prophylactic and therapeutic models. And then, we next looked at the induction of Treg in the inflamed skin. Naturally occurring $CD4^+CD25^+$ Treg are characterized by the expression of Foxp3 [10, 27]. Skin sections were stained with anti-Foxp3 mAb, and examined with a fluorescent microscope. As shown in Fig. 6b, $Foxp3^+$ cells were increased in the Ag85B-treated mice.

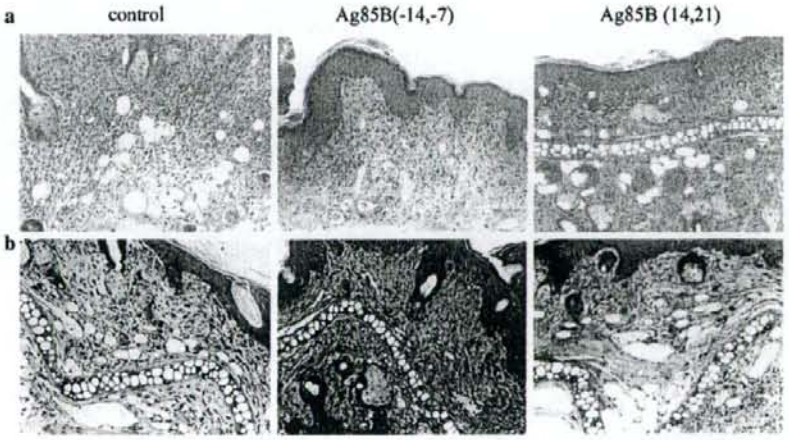

Fig. 3 Histopathological features of skin lesions. Skin was taken on day 35, paraffin embedded sections were stained with **a** hematoxylin and eosin or **b** truidine blue. OX-challenged mice showed epidermal hyperplasia along with strong intradermal inflammatory cell infiltration; whereas Ag85B DNA significantly reduced the inflammatory changes

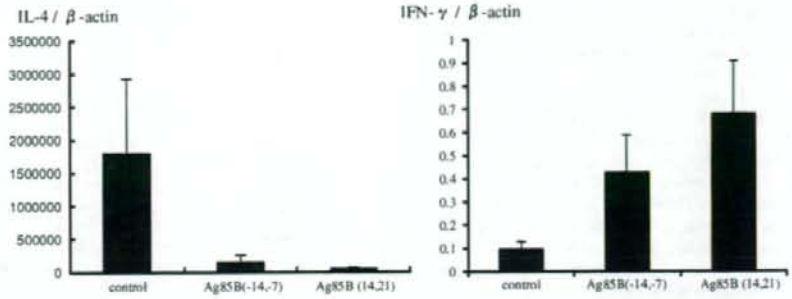

Fig. 4 mRNA expression in the ear on day 35. In order to clarify the expression of cytokine mRNA, quantitative PCR was performed by using specific primers and probes for IL-4 and IFN-γ. The expression of IL-4 mRNA was reduced in Ag85B-treated mice compared with placebo-treated mice. On the other hand, mRNA expression of IFN-γ was significantly increased in Ag85B mice

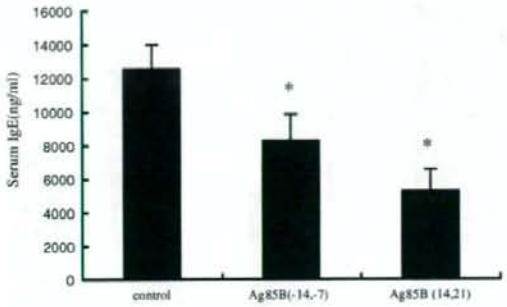

Fig. 5 Serum IgE concentrations. Serum IgE levels were measured on day 35 in control, Ag85B DNA IP (−14, −7), or Ag85B DNA IP (14, 21) mice. The columns and error bars represent mean ± SEM. $^*P < 0.05$. Administration of Ag85B reduced IgE level

Discussion

Human immune system responds to exogenous microorganisms for self-protection. These responses lead to Th1 and/ or Th2 type cytokine secretion depending on the nature of stimuli. AD is a chronic dermatitis characterized by a Th2-type immune responses that causes elevation of IgE. On the other hand, some bacterial infections including *Mycobacterium* species elicits strong Th1-type responses. Inducers of Th1 type immune response may be used as immuno-modulator having therapeutic effects against allergic disease elicited by Th2-type immune responses. Mycobacteria may affect atopic disorders by correction of the immune response from Th2 to Th1. Erb et al. reported that *M. bovis* (BCG) suppresses airway eosinophilia and associated local IL-5 production by inducing Th1-mediated response [9]. Furthermore, recent studies suggested that mycobacteria induce not only Th cells providing Th1 type immune responses but also Treg cells. In an animal model of allergy, the immunomodulatory effects of *M. vaccae* was found to be mediated by allergen-specific regulatory T lymphocytes [37], and oral administration of *M. vaccae* inhibited pulmonary allergic inflammation by induction of IL-10 [14].

Alive BCG vaccination has been used for prevention of tuberculosis. The use of *Mycobacterium* for immunomodulation requires repeated exposures to the immune system. However, repeated alive BCG vaccination is contraindicated. For human therapeutic application, it needs intradermal or intramuscular injection for vaccination. Unfortunately, cutaneous vaccination with *Mycobacterium* species commonly produces granulomatous formation leading to recalcitrant ulcers. We need to develop Th1 type immunomodulating system that induces no granulomatous reaction, if species of mycobacteria are tried to use for human. The Ag85B protein is a main component of the cell wall of mycobacteria such as *M. tuberculosis and M. kansasii* [4]; this Ag85B is known as a strong Th1 inducer in vitro [17, 18]. Experiments using plasmid DNA encoding Ag85B has been previously reported. This Ag85B is able to protect against *M. tuberculosis* even in Balb/c mice [33]. Intraperitoneal administration of Ag85B DNA inhibits granulomatous changes or adhesive reaction of intraperitoneal organs in mice (data not shown). As a preliminary study, Ag85B DNA was intradermally injected in the skin of mice skin. No ulcerative changes were observed in vaccinated areas of the skin (data not shown).

In our present study, we evaluated the efficacy of DNA encoding Ag85B for inducing Th1- and Treg-type immune response in OX-induced acute phase dermatitis. Repeated applications of OX in mice ears caused Th2-type dominant dermatitis, which mimic most of the characteristic features of AD [16, 19, 20, 32]. We first investigated whether the application of Ag85B corrects the immune response from a type Th2 one to a type Th1 response. Our results showed that Ag85B successfully ameliorates Th2-cytokine dominant immediate type reaction in the skin lesions in both prophylactic and therapeutic models of the disease. In Ag85B-treated AD skin lesion, the ear swelling was significantly reduced compared to placebo-treated animals. Administration of Ag85B DNA suppressed histological abnormalities caused by atopic inflammations such as inflammatory cell infiltration, epidermal hyperplasia, and severe edema. The presence of mast cells in the skin lesion is closely associated with Th2-type dermatitis; the number of mast cells was

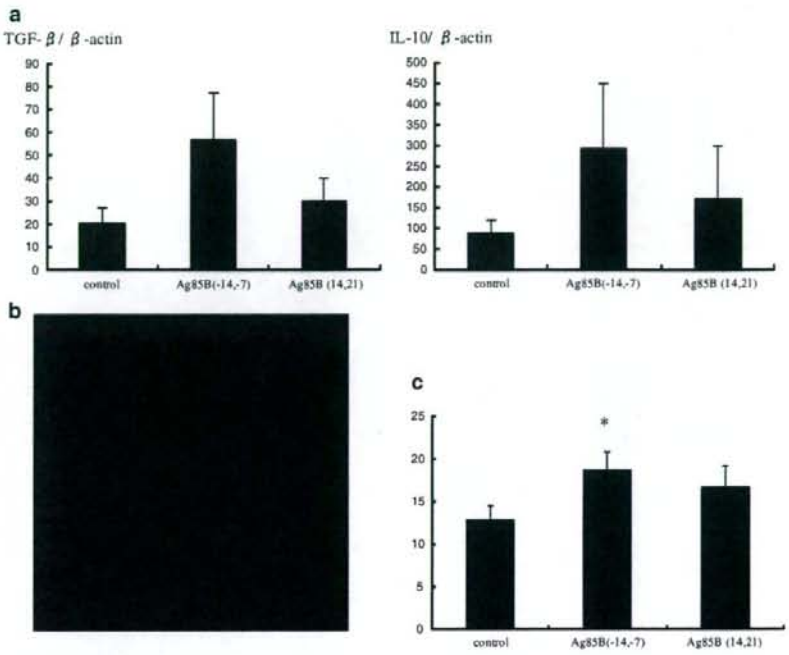

Fig. 6 **a** mRNA expression in the ear on day 35. Quantitative PCR was performed by using specific primers and probes for IL-10 and TGF-β. Both TGF-β and IL-10 were increased in the Ag85B-treated mice. **b** Foxp3$^+$ cells were clearly observed with confocal microscopy. **c** The number of Foxp3$^+$ cells per HPF was counted in five nonconsecutive fields, and Foxp3$^+$ cells were found to be increased in Ag85B-treated mice

increased in OX-treated control animals as expected; however, the number of mast cells was decreased in Ag85B-treated mice compared with controls. Enhancement of the expression of IFN-γ mRNA was significant in Ag85B-treated AD mice compared with placebo-treated animals. The expression of IL-4 mRNA were suppressed in Ag85B-treated mice compared to placebo-treated controls (Fig. 4). In addition, serum IgE levels were significantly suppressed in Ag85B treated mice compared with placebo-treated mice. These finding demonstrates that administration of Ag85B DNA significantly inhibited the development of Th2-cytokine dominant atopic inflammation by inducing Th1-type immune response.

We also examined the potential of Ag85B to induce Treg cell responses. TGF-β and IL-10 have been described as critical regulatory cytokines produced by Treg [11]. Heat-killed *M. vaccae* induces regulatory T cells that secrete IL-10 and TGF-β [37]. *M. vaccae* also induces a population of CD11$^+$ cells characterized by an increased expression of regulatory cytokines including IL-10 and TGF-β[1]. Treg cells are developed mainly in the presence of IL-10 and TGF-β [13]. More recently, Inoue and Aramaki reported that topical application of CpG-Oligodeoxynucleotides induces Foxp3$^+$ Treg in skin lesions of AD model mice in association with elevation of TGF-β[15]. Depletion of CD4$^+$CD25$^+$Treg from the peripheral blood of healthy individuals enhances proliferation of Th2 in response to various allergens [6, 23]. The mechanisms of the suppressive activity of Treg depend on cell-to-cell contact, and there is evidence for the involvement of IL-10 and TGF-β[2, 3, 26]. In this study, we have shown elevated expression of TGF-β and IL-10 in Ag85B-treated mice (Fig. 6a), and Foxp3$^+$ Treg was increased in the Ag85B-treated skin (Fig. 6b). We assume that the therapeutics capability of Ag85B is related to the induction of Foxp3$^+$Treg and Th1-type immune response.

In brief, in this study we have shown the usefulness of plasmid DNA of Ag85B for the amelioration of Th1/Th2 imbalance and for the generation of Treg cells. The observations suggest that Ag85B may be useful for the prevention and treatment of atopic disorders.

Acknowledgments This work was supported in part by Health Science Research Grants from the Ministry of Health, Labor and Welfare of Japan and the Ministry of Education, Culture, Sports, Science and Technology of Japan, Grants-in-Aid for Scientific Research and Grants-in-Aid for Core Research Evolutional Science and Technology.

Conflicts of interest statement None.

References

1. Adams VC, Hunt JR, Martinelli R, Palmer R, Rook GA, Brunet LR (2004) *Mycobacterium vaccae* induces a population of pulmonary CD11c+ cells with regulatory potential in allergic mice. Eur J Immunol 34:631–638

2. Akdis M, Verhagen J, Taylor A, Karamloo F, Karagiannidis C, Crameri R, Thunberg S, Deniz G, Valenta R, Fiebig H, Kegel C, Disch R, Schmidt-Weber CB, Blaser K, Akdis CA (2004) Immune responses in healthy and allergic individuals are characterized by a fine balance between allergen-specific T regulatory 1 and T helper 2 cells. J Exp Med 199:1567–1575
3. Asseman C, Mauze S, Leach MW, Coffman RL, Powrie F (1999) An essential role for interleukin 10 in the function of regulatory T cells that inhibit intestinal inflammation. J Exp Med 190:995–1004
4. Belisle JT, Vissa VD, Sievert T, Takayama K, Brennan PJ, Besra GS (1997) Role of the major antigen of *Mycobacterium tuberculosis* in cell wall biogenesis. Science 276:1420–1422
5. Burney PG, Chinn S, Rona RJ (1990) Has the prevalence of asthma increased in children? Evidence from the national study of health and growth 1973–86. BMJ 300:1306–1310
6. Cavani A, Nasorri F, Ottaviani C, Sebastiani S, De Pita O, Girolomoni G (2003) Human CD25+ regulatory T cells maintain immune tolerance to nickel in healthy, nonallergic individuals. J Immunol 171:5760–5768
7. Cookson WO, Moffatt MF (1997) Asthma: an epidemic in the absence of infection? Science 275:41–42
8. Del Prete G (1992) Human Th1 and Th2 lymphocytes: their role in the pathophysiology of atopy. Allergy 47:450–455
9. Erb KJ, Holloway JW, Sobeck A, Moll H, Le Gros G (1998) Infection of mice with *Mycobacterium bovis*-Bacillus Calmette-Guerin (BCG) suppresses allergen-induced airway eosinophilia. J Exp Med 187:561–569
10. Fontenot JD, Gavin MA, Rudensky AY (2003) Foxp3 programs the development and function of CD4+CD25+ regulatory T cells. Nat Immunol 4:330–336
11. Groux H, O'Garra A, Bigler M, Rouleau M, Antonenko S, de Vries JE, Roncarolo MG (1997) A CD4+ T-cell subset inhibits antigen-specific T-cell responses and prevents colitis. Nature 389:737–742
12. Herz U, Gerhold K, Gruber C, Braun A, Wahn U, Renz H, Paul K (1998) BCG infection suppresses allergic sensitization and development of increased airway reactivity in an animal model. J Allergy Clin Immunol 102:867–874
13. Horwitz DA, Zheng SG, Gray JD (2003) The role of the combination of IL-2 and TGF-beta or IL-10 in the generation and function of CD4+ CD25+ and CD8+ regulatory T cell subsets. J Leukoc Biol 74:471–478
14. Hunt JR, Martinelli R, Adams VC, Rook GA, Brunet LR (2005) Intragastric administration of *Mycobacterium vaccae* inhibits severe pulmonary allergic inflammation in a mouse model. Clin Exp Allergy 35:685–690
15. Inoue J, Aramaki Y (2007) Suppression of skin lesions by transdermal application of CpG-oligodeoxynucleotides in NC/Nga mice, a model of human atopic dermatitis. J Immunol 178:584–591
16. Inoue Y, Isobe M, Shiohara T, Goto Y, Hayashi H (2002) Protective and curative effects of topically applied CX-659S, a novel diaminouracil derivative, on chronic picryl chloride-induced contact hypersensitivity responses. Br J Dermatol 147:675–682
17. Kariyone A, Higuchi K, Yamamoto S, Nagasaka-Kametaka A, Harada M, Takahashi A, Harada N, Ogasawara K, Takatsu K (1999) Identification of amino acid residues of the T-cell epitope of *Mycobacterium tuberculosis* alpha antigen critical for Vbeta11(+) Th1 cells. Infect Immun 67:4312–4319
18. Kariyone A, Tamura T, Kano H, Iwakura Y, Takeda K, Akira S, Takatsu K (2003) Immunogenicity of Peptide-25 of Ag85B in Th1 development: role of IFN-gamma. Int Immunol 15:1183–1194
19. Kitagaki H, Fujisawa S, Watanabe K, Hayakawa K, Shiohara T (1995) Immediate-type hypersensitivity response followed by a late reaction is induced by repeated epicutaneous application of contact sensitizing agents in mice. J Invest Dermatol 105:749–755
20. Kitagaki H, Ono N, Hayakawa K, Kitazawa T, Watanabe K, Shiohara T (1997) Repeated elicitation of contact hypersensitivity induces a shift in cutaneous cytokine milieu from a T helper cell type 1 to a T helper cell type 2 profile. J Immunol 159:2484–2491
21. Kitagaki H, Kimishima M, Teraki Y, Hayakawa J, Hayakawa K, Fujisawa S, Shiohara T (1999) Distinct in vivo and in vitro cytokine profiles of draining lymph node cells in acute and chronic phases of contact hypersensitivity: importance of a type 2 cytokine-rich cutaneous milieu for the development of an early-type response in the chronic phase. J Immunol 163:1265–1273
22. Kuromatsu I, Matsuo K, Takamura S, Kim G, Takebe Y, Kawamura J, Yasutomi Y (2001) Induction of effective antitumor immune responses in a mouse bladder tumor model by using DNA of an alpha antigen from mycobacteria. Cancer Gene Ther 8:483–490
23. Ling EM, Smith T, Nguyen XD, Pridgeon C, Dallman M, Arbery J, Carr VA, Robinson DS (2004) Relation of CD4+CD25+ regulatory T-cell suppression of allergen-driven T-cell activation to atopic status and expression of allergic disease. Lancet 363:608–615
24. McKnight AJ, Zimmer GJ, Fogelman I, Wolf SF, Abbas AK (1994) Effects of IL-12 on helper T cell-dependent immune responses in vivo. J Immunol 152:2172–2179
25. Overbergh L, Valckx D, Waer M, Mathieu C (1999) Quantification of murine cytokine mRNAs using real time quantitative reverse transcriptase PCR. Cytokine 11:305–312
26. Powrie F, Carlino J, Leach MW, Mauze S, Coffman RL (1996) A critical role for transforming growth factor-beta but not interleukin 4 in the suppression of T helper type 1-mediated colitis by CD45RB(low) CD4+ T cells. J Exp Med 183:2669–2674
27. Sakaguchi S, Sakaguchi N, Shimizu J, Yamazaki S, Sakihama T, Itoh M, Kuniyasu Y, Nomura T, Toda M, Takahashi T (2001) Immunologic tolerance maintained by CD25+ CD4+ regulatory T cells: their common role in controlling autoimmunity, tumor immunity, and transplantation tolerance. Immunol Rev 182:18–32
28. Shirakawa T, Enomoto T, Shimazu S, Hopkin JM (1997) The inverse association between tuberculin responses and atopic disorder. Science 275:77–79
29. Swain SL, Weinberg AD, English M, Huston G (1990) IL-4 directs the development of Th2-like helper effectors. J Immunol 145:3796–3806
30. Takamura S, Matsuo K, Takebe Y, Yasutomi Y (2005) Ag85B of mycobacteria elicits effective CTL responses through activation of robust Th1 immunity as a novel adjuvant in DNA vaccine. J Immunol 175:2541–2547
31. Takatsu K, Kariyone A (2003) The immunogenic peptide for Th1 development. Int Immunopharmacol 3:783–800
32. Tamura T, Matsubara M, Hasegawa K, Ohmori K, Karasawa A (2005) Olopatadine hydrochloride suppresses the rebound phenomenon after discontinuation of treatment with a topical steroid in mice with chronic contact hypersensitivity. Clin Exp Allergy 35:97–103
33. Teixeira FM, Teixeira HC, Ferreira AP, Rodrigues MF, Azevedo V, Macedo GC, Oliveira SC (2006) DNA vaccine using *Mycobacterium bovis* Ag85B antigen induces partial protection against experimental infection in BALB/c mice. Clin Vaccine Immunol 13:930–935
34. Ulmer JB, Montgomery DL, Tang A, Zhu L, Deck RR, DeWitt C, Denis O, Orme I, Content J, Huygen K (1998) DNA vaccines against tuberculosis. Novartis Found Symp 217:239–246 discussion 246–253
35. Yazdanbakhsh M, Kremsner PG, van Ree R (2002) Allergy, parasites, and the hygiene hypothesis. Science 296:490–494
36. Zhu D, Jiang S, Luo X (2005) Therapeutic effects of Ag85B and MPT64 DNA vaccines in a murine model of *Mycobacterium tuberculosis* infection. Vaccine 23:4619–4624
37. Zuany-Amorim C, Sawicka E, Manlius C, Le Moine A, Brunet LR, Kemeny DM, Bowen G, Rook G, Walker C (2002) Suppression of airway eosinophilia by killed *Mycobacterium vaccae*-induced allergen-specific regulatory T-cells. Nat Med 8:625–629

Prior Immunization with Severe Acute Respiratory Syndrome (SARS)-Associated Coronavirus (SARS-CoV) Nucleocapsid Protein Causes Severe Pneumonia in Mice Infected with SARS-CoV[1]

Fumihiko Yasui,* Chieko Kai,[‡] Masahiro Kitabatake,[2]* Shingo Inoue,[‖] Misako Yoneda,[‡] Shoji Yokochi,*[§] Ryoichi Kase,* Satoshi Sekiguchi,* Kouichi Morita,[‡] Tsunekazu Hishima,[¶] Hidenori Suzuki,[†] Katsuo Karamatsu,[#] Yasuhiro Yasutomi,[#] Hisatoshi Shida,** Minoru Kidokoro,[††] Kyosuke Mizuno,[‡‡] Kouji Matsushima,[§] and Michinori Kohara[3]*

The details of the mechanism by which severe acute respiratory syndrome-associated coronavirus (SARS-CoV) causes severe pneumonia are unclear. We investigated the immune responses and pathologies of SARS-CoV-infected BALB/c mice that were immunized intradermally with recombinant vaccinia virus (VV) that expressed either the SARS-CoV spike (S) protein (LC16m8rVV-S) or simultaneously all the structural proteins, including the nucleocapsid (N), membrane (M), envelope (E), and S proteins (LC16m8rVV-NMES) 7–8 wk before intranasal SARS-CoV infection. The LC16m8rVV-NMES-immunized group exhibited as severe pneumonia as the control groups, although LC16m8rVV-NMES significantly decreased the pulmonary SARS-CoV titer to the same extent as LC16m8rVV-S. To identify the cause of the exacerbated pneumonia, BALB/c mice were immunized with recombinant VV that expressed the individual structural proteins of SARS-CoV (LC16mOrVV-N, -M, -E, -S) with or without LC16mOrVV-S (i.e., LC16mOrVV-N, LC16mOrVV-M, LC16mOrVV-E, or LC16mOrVV-S alone or LC16mOrVV-N + LC16mOrVV-S, LC16mOrVV-M + LC16mOrVV-S, or LC16mOrVV-E + LC16mOrVV-S), and infected with SARS-CoV more than 4 wk later. Both LC16mOrVV-N-immunized mice and LC16mOrVV-N + LC16mOrVV-S-immunized mice exhibited severe pneumonia. Furthermore, LC16mOrVV-N-immunized mice upon infection exhibited significant up-regulation of both Th1 (IFN-γ, IL-2) and Th2 (IL-4, IL-5) cytokines and down-regulation of anti-inflammatory cytokines (IL-10, TGF-β), resulting in robust infiltration of neutrophils, eosinophils, and lymphocytes into the lung, as well as thickening of the alveolar epithelium. These results suggest that an excessive host immune response against the nucleocapsid protein of SARS-CoV is involved in severe pneumonia caused by SARS-CoV infection. These findings increase our understanding of the pathogenesis of SARS. *The Journal of Immunology*, **2008, 181: 6337–6348.**

From November 2002 to July 2003, an outbreak of severe acute respiratory syndrome (SARS),[4] which originated in China, spread worldwide, resulting in 8098 cases with 774 deaths (http://www.who.int/csr/sars/country/en/index.html). Patients with SARS usually develop high fever followed by severe clinical symptoms, which include acute respiratory distress syndrome with diffuse alveolar damage, and ultimately death. A novel type of coronavirus (CoV), termed SARS-associated CoV (SARS-CoV), was identified as the etiologic agent of SARS (1–3). The genome of SARS-CoV is a single strand of positive-sense RNA of ~30 kb in length with 14 putative open reading frames, which encode nonstructural replicase polyproteins and several structural proteins, including spike (S), envelope (E), membrane (M), and nucleocapsid (N) proteins (4). The S protein of SARS-CoV, like the S proteins of other CoVs, plays an important role in the first step of viral infection by binding to a host cell receptor. Angiotensin-converting enzyme 2 was identified as the host receptor for SARS-CoV (5). Angiotensin-converting enzyme 2 is abundantly expressed in the epithelia of the lung and small intestine and may mediate SARS-CoV entry in humans (6). Although intensive investigations rapidly unraveled the sequence of the SARS-CoV genome and its receptor in humans, the precise molecular mechanism underlying the development of SARS is not fully understood.

The possible roles of host anti-SARS-CoV immune responses have been suggested in severe clinical cases. The uncontrolled release of immune mediators, called a "cytokine storm," has been

*Department of Microbiology and Cell Biology, [†]Laboratory of Electron Microscopy, The Tokyo Metropolitan Institute of Medical Science, [‡]Laboratory Animal Research Center, The Institute of Medical Science, [§]Department of Molecular Preventive Medicine, School of Medicine, The University of Tokyo, and [¶]Department of Pathology, Tokyo Metropolitan Komagome Hospital, Tokyo, Japan; [‖]Department of Virology, Institute of Tropical Medicine, Nagasaki University, Nagasaki, Japan; [#]Laboratory of Immunoregulation and Vaccine Research, Tsukuba Primate Research Center, National Institute of Biomedical Innovation, Ibaraki, Japan; **Division of Molecular Virology, Institute for Genetic Medicine, Hokkaido University, Sapporo, Japan; [††]Third Department of Virology, National Institute of Infectious Diseases, Musashimurayama, Japan; and [‡‡]The Chemo-Sero-Therapeutic Research Institute, Kumamoto, Japan

Received for publication January 23, 2008. Accepted for publication August 23, 2008.

The costs of publication of this article were defrayed in part by the payment of page charges. This article must therefore be hereby marked *advertisement* in accordance with 18 U.S.C. Section 1734 solely to indicate this fact.

[1] This study was supported in part by a Grant for Research on Emerging and Re-emerging Infectious Diseases from the Ministry of Health, Labor and Welfare, Japan, by the 21st Century Centers of Excellence program on Global Strategies for Control of Tropical and Emerging Infectious Diseases at Nagasaki University, and by the Ministry of Education, Culture, Sports, Science and Technology of Japan. Strategic cooperation to control emerging and re-emerging infections is funded by the Special Co-ordination Fund for Promoting Science and Technology of the Ministry of Education, Culture, Sports, Science and Technology.

[2] Current address: Department of Immunology, Graduate School of Medicine, Kumamoto University, 1-1-1 Honjo, Kumamoto, 860-8556, Japan.

[3] Address correspondence and reprint requests to Dr. Michinori Kohara, Department of Microbiology and Cell Biology, The Tokyo Metropolitan Institute of Medical Science, 3-18-22 Honkomagome, Bunkyo-ku, Tokyo 113-8613, Japan. E-mail address: kohara-mc@igakuken.or.jp

[4] Abbreviations used in this paper: SARS, severe acute respiratory syndrome; CoV, coronavirus; VV, vaccinia virus; HA, hemagglutinin; MOI, multiplicity of infection; VLP, virus-like particle; $TCID_{50}$, tissue culture ID_{50}.

implicated in the pathogenesis of SARS. However, the cytokine profiles of SARS patient sera do not correlate with the severity of pneumonia because of their diversity. For example, Jones et al. (7) have reported a decreased number of IL-2-, IL-4-, IL-10-, and IL-12-producing cells in SARS-CoV-infected patients. In contrast, Wong et al. (8) have demonstrated increased production of IFN-γ, IL-1, IL-6, and IL-12 p70, but not of IL-2, IL-4, IL-10 or TNF-α, which is consistent with a Th1 response. The data from these adult patients with SARS show no clear trend toward either a Th1 or Th2 bias. These results might be related to patient anamnesis. Therefore, the development of animal models for SARS is needed to understand the pathogenesis of SARS. Non-human primates, mice, ferrets, and hamsters have been found to support the replication of SARS-CoV (9–14). However, an animal model that mimics the clinical symptoms and pathology observed in SARS patients has not been reported to date. Recently, Roberts et al. (15) reported that aged BALB/c mice (older than 12 mo) exhibited high and prolonged levels of viral replication, signs of clinical symptoms, and histopathologic changes in the lung. Aged BALB/c mice represent a conventional animal model that mimics the findings in elderly SARS patients, many of whom exhibit severe disease requiring intensive care and ventilation support, as well as increased mortality.

In the present study, we investigated the pulmonary immune responses and pathologies of intranasally SARS-CoV-infected BALB/c mice older than 6 mo of age that were previously immunized with SARS-CoV structural proteins using vaccinia virus (VV) vectors, by measuring various cytokine mRNAs and histopathologies of the lungs.

Materials and Methods

Cells and viruses

RK13 cells (CCL-37) from the American Type Culture Collection (ATCC) and Vero E6 cells (CRL-1586) from ATCC were cultured in MEM (Nissui Pharmaceutical) that contained 5% FCS. To generate recombinant VV LC16m8, which expresses the structural proteins of SARS-CoV, primary rabbit kidney cell cultures were prepared by overnight digestion with 100 PU/ml dispase (Sanko Jun-yaku) of kidneys extirpated from 7-day-old inbred JW rabbits (Kitayama Labs). The cells were grown in T175 flasks in lactalbumin medium with Hank's salts (LH) that contained 5% FCS, 100 U/ml penicillin, and 100 μg/ml streptomycin. When the cell confluency was ~50%, the culture medium was replaced with lactalbumin medium with Eagle's salts (LE) that contained 5% FCS, 100 U/ml penicillin, and 100 μg/ml streptomycin. SARS-CoV Vietnam/NB-04/2003 strain, which was isolated from the throat wash fluid of one patient (16), was provided by Dr. M. Quynh Le. VVs LC16m8 (m8) and LC16mO (mO) were provided by the Chemo-Sero-Therapeutic Research Institute (Kumamoto, Japan). All work using SARS-CoV was performed in BioSafety Level 3 facilities by personnel wearing powered air-purifying respirators (Shigematsu Works).

Generation of recombinant VV

To generate a pBR322-based plasmid vector (pBMSF) for homologous recombination into the hemagglutinin (HA) locus of m8, we cloned the HA gene, which contained the ATI/p7.5 synthetic hybrid promoter, from the pSFJ1–10 plasmid and inserted it into the pBM vector, which was reconstructed in our laboratory. Full-length cDNAs for the SARS-CoV nucleocapsid (N), membrane (M), and envelope (E) proteins were cloned from the Vietnam/NB-04/2003 strain of SARS-CoV by RT-PCR (16). Full-length SARS-CoV spike (S) protein gene was prepared from pSFJ1-10-SARS-S, which is described in our previous report (17). Next, the genes that encode the SARS-CoV structural proteins were ligated by inserting internal ribosomal entry site sequence of hepatitis C virus (genotypes 2a and 1b/2b) fused with the 2A sequence of foot and mouth disease virus and *Thosea asigna* virus or encephalomyocarditis virus by PCR (see Fig. 1*A*). The generated DNA fragment was digested with *Eco*RI and inserted downstream of the ATI/p7.5 hybrid promoter of pBR322-based plasmid vector pBMSF, thereby generating pBMSF-SARS-NMES. The pBMSF-SARS-NMES plasmid was linearized with *Pvu*I, and transfected into primary rabbit kidney cells that had been infected with m8 at a multiplicity of infection (MOI) of 10. After 36 h, the virus-cell mixture were harvested by scraping, and frozen at −80°C until use. The resulting HA-negative recombinant viruses were purified as previously described (17), and named m8rVV-NMES. Furthermore, recombinant mO that expressed the SARS-CoV N, M, or E protein with a six histidine tag at the C terminus was generated (mOrVV-NHis, mOrVV-MHis, and mOrVV-EHis), as was mO that expressed six histidine-tagged S protein (mOrVV-SHis), as previously described (17).

Western blot analysis

Vero E6 cells were infected with m8rVV-NMES at an MOI of 5. After 18 h, the cells were lysed with lysis buffer (10 mM Tris (pH 7.4), 150 mM NaCl, 1% SDS, 0.5% Nonidet P-40, protease inhibitor cocktail). The cell lysates (30 μg) were resolved by SDS-PAGE and transferred to a polyvinylidene difluoride membrane (Immobilon-P; Millipore). After blocking the membranes with 5% skim milk solution at room temperature for 1 h, the membrane was incubated with polyclonal Abs against the N, M, E, or S protein. Vero E6 cell lysates infected with mOrVV-NHis, mOrVV-MHis, mOrVV-EHis, or mOrVV-SHis was used as positive controls. We used the anti-S polyclonal Abs described in our previous study (17). Polyclonal Abs against N and E proteins were prepared from rabbit sera immunized with KLH-conjugated N peptide (residues aa 250–263) and E peptide (residues aa 61–73). Polyclonal Abs against the M protein were provided by Dr. Mizutani (National Institute of Infectious Diseases, Musashimurayama, Tokyo). We purified the IgG fractions of these antisera using the protein A Ampure PA kit (Amersham Biosciences). After washing with TBS that contained 0.1% Tween 20 (TBST), the membranes were reacted with HRP-conjugated $F(ab')_2$ of anti-rabbit IgG (GE Healthcare). Each specific protein band was visualized using the ECL system (GE Healthcare).

Indirect immunofluorescence analysis

Vero E6 cells were infected with m8rVV-NMES at an MOI of 5 at 30°C for 4 h. The cells were washed with PBS and fixed with cold acetone/methanol (1/1) mixture for 10 min. After blocking with TNB blocking buffer (NEN Life Science Products) at room temperature for 1 h, the fixed cells were incubated with polyclonal Abs against the N, M, or E protein or mAb against the S protein (designated as anti-S-His protein, clone no. 13B8), which was originally prepared in our laboratory, at 4°C overnight. After washing, the cells were incubated with Alexa Fluor 488-conjugated anti-rabbit IgG or mouse IgG Ab at room temperature for 1 h. Nuclei were stained with DAPI (4′,6-diamidino-2-phenylindole). Fluorescence images were acquired using a confocal microscope (LSM510 META; Carl Zeiss).

Confirmation of SARS-CoV-like particle formation

RK13 cells were cultured in 150-mm dishes, and then infected with m8rVV-NMES at an MOI of 5. After 48 h of incubation, the culture supernatants were collected and centrifuged to remove cell debris at 3000 rpm for 30 min at 4°C. The supernatants were concentrated ~100-fold using the Pellicon XL (cut off molecular weight 3×10^5; Millipore). The isolation of virus-like particles (VLP) was performed as previously described, with a slight modification (18). Briefly, the concentrated supernatant was placed on 60% (w/w) sucrose cushion and centrifuged at 4.0×10^4 rpm for 5 h. The opalescent band was collected and centrifuged in a 20–60% (w/w) sucrose gradient at 2.7×10^4 rpm for 4 h, and then divided into 20 fractions. The protein content of each fraction was determined with the DC protein assay kit (Bio-Rad). The 20 μl of each fraction were separated by SDS-PAGE (7.5%, 10%, or 15% polyacrylamide gel), and transferred onto a polyvinylidene difluoride membrane. The membrane was incubated with mAb against S protein (13B8), mAb against N protein (IMG-654; Imgenex) or polyclonal Abs against the M or E protein. After washing, the membranes were reacted and visualized as described. The VLPs in the concentrated culture supernatant were visualized using transmission electron microscopy. For immunogold staining, VLPs were loaded onto a collodion-coated electron microscopy grid for 5 min. After the removal of excess sample solution, polyclonal Ab against S protein was added onto the grid and incubated at room temperature for 1 h. The grids were washed six times with Sorensen's phosphate buffer at room temperature and incubated with 5-nm gold-conjugated anti-rabbit IgG for 1 h. After washing with Sorensen's phosphate buffer for 10 s, the samples were stained with 2% phosphotungstic acid for 1 min. After draining off the excess phosphotungstic acid, the samples were observed under the electron microscopy.

Immunization of rabbits with m8rVV-NMES

Groups of three New Zealand White rabbits (SLC) were immunized intradermally with 1×10^8 PFU/body of m8rVV-NMES or with 1×10^8 PFU/body of m8, at 0 and 6 wk. Sera were collected at the indicated time